Potential sand sources for the dune fields in Noachis Terra, Mars

Lori K. Fenton

Department of Geology, Arizona State University, Tempe, Arizona, USA

Received 21 March 2005; revised 27 June 2005; accepted 11 August 2005; published 22 November 2005.

[1] No sand transport pathways are visible in a study performed in Noachis Terra, a 60° × 35° region in the southern highlands of Mars known for its many intracrater dune fields. Detailed studies were performed of five areas in Noachis Terra, using Mars Orbiter Camera (MOC) wide-angle mosaics, Thermal Emission Imaging System (THEMIS) daytime and nighttime infrared mosaics, MOLA digital elevation and shaded relief maps, and MOC narrow-angle images. The lack of observable sand transport pathways suggests that such pathways are very short, ruling out a distant source of sand. Consistent dune morphology and dune slipface orientations across Noachis Terra suggest formative winds are regional rather than local (e.g., crater slope winds). A sequence of sedimentary units was found in a pit eroded into the floor of Rabe Crater, some of which appear to be shedding dark sand that feeds into the Rabe Crater dune field. The visible and thermal characteristics of these units are similar to other units found across Noachis Terra, leading to the hypothesis that a series of region-wide depositional events occurred at some point in the Martian past and that these deposits are currently exposed by erosion in pits on crater floors and possibly on the intercrater plains. Thus the dune sand sources may be both regional and local: sand may be eroding from a widespread source that only outcrops locally. Sand-bearing layers that extend across part or all of the intercrater plains of Noachis Terra are not likely to be dominated by loess or lacustrine deposits; glacial and/or volcanic origins are considered more plausible.

Citation: Fenton, L. K. (2005), Potential sand sources for the dune fields in Noachis Terra, Mars, *J. Geophys. Res.*, *110*, E11004, doi:10.1029/2005JE002436.

1. Introduction

[2] On any planetary body, the patterns of aeolian deposition, material transport, and erosion are a record of the various processes acting upon the planetary surface. On Earth, these processes are dictated by the current and previous states of climate, topography, water, and vegetation. On Mars, where tectonics and liquid water are minimal in the present epoch and vegetation is nonexistent, it is climate shifts that most influence changes in aeolian depositional and erosional patterns. Dune fields and the sand transport pathways that feed them are particularly sensitive to changes in climate, which can shift patterns of wind energy, wind direction, and moisture, which in turn modify dune morphology and the activity of the transport pathways. Gaining an understanding of how the sand transport pathways carry sand from their source location to dune fields can provide insights not only on patterns of deposition and erosion, but also on recent climate change.

[3] The purpose of this work is to seek out sand transport pathways in Noachis Terra on Mars. The characteristics of such pathways have the potential to reveal much about aeolian, climatic, and sedimentary processes in the southern highlands, such as how far the source materials have traveled, the current activity level of any such pathways, and the spatial patterns and processes of erosion that created the dune sand. In this work, no large sand transport pathways are visible in any data set. However, small local sources that are presently active are located near some dune fields. These local sand sources consist of eroding sedimentary layers within a sequence of strata with characteristic variations in texture and thermal properties. This sequence appears to be repeated in different places across Noachis Terra, but it is best exposed in the walls of a pit in Rabe Crater. It is possible that these layers are erosional remnants of a once widespread sequence of layers that extended across all or parts of Noachis Terra.

1.1. Examples of Terrestrial Work

[4] The study of terrestrial sand transport pathways is extensive, so only a few examples are described here to illustrate some of the research that inspired this study. In some places, sand is thought to have traveled across distances greater than 1000 km from source to sink (i.e., dune field) [*Fryberger and Ahlbrandt*, 1979]. Dune orientations in the Sahara and Australian deserts have been analyzed, and they appear to correspond to large-scale wind circulation patterns [e.g., *Mainguet*, 1978; *Mainguet and El-Baz*, 1986]. Several sets of connected transport pathways have been found crossing eastward across the Mojave Desert in the southwestern United States, forming sand ramps to climb over mountain ranges and locally accumulating in topographic lows as dune fields [*Zimbelman et al.*,

0148-0227/05/2005JE002436$09.00

1995; *Clarke and Rendell*, 1998]. Dune morphology has also been studied to understand wind circulation patterns under a different climatic regime. For example, dune fields in both Europe [e.g., *Isarin et al.*, 1997] and North America [e.g., *Muhs et al.*, 1996] that date to the Late Pleistocene but were subsequently reworked during later intervals (both glacial and interglacial) provide a record of the local wind regime that may be compared to present-day winds.

[5] Combining multiple data sets has proved even more useful than using any one technique alone. For example, *Ramsey et al.* [1999] used infrared spectroscopy and spacecraft imagery to confirm that most of the sand in the Kelso Dunes in the Mojave Desert originated upwind from the Mojave River (on a pathway also identified in work by *Zimbelman et al.* [1995]), but that some minerals present in the dunes indicate an additional minor local source from the adjacent mountains. Combining analysis of morphology and luminescence dating of dunes in the western Sahara Desert in Mauritania, *Lancaster et al.* [2002] found three generations of dunes, each with a distinctive size, orientation, and age. These corresponding characteristics suggest that different climate states are reflected in the varying morphologies of the dunes. *Kocurek and Lancaster* [1999] used estimates of sediment supply, transport rate, and transport capacity of the wind to characterize the sediment state of the Kelso Dunes, delimiting phases of aeolian construction. Their method provides a good conceptual model that is applicable to aeolian systems on any planetary body.

[6] The above examples are but a few of the terrestrial studies that are beginning to tie dune morphology and sand transport pathways to recent climate change. Although studies combining morphology based on spacecraft images with other techniques provide more information than studies of imagery alone, it is remarkable how well the image studies correspond to what is already known about terrestrial wind patterns and climate states. The vast quantity of remote sensing data of Mars lends itself well to this sort of study, even though results are not yet verifiable with fieldwork.

1.2. Deposition and Erosion on Mars

[7] Without plate tectonics to recycle sediments in the planetary interior, the only sink for dust and sand on Mars is the surface itself. The Martian surface shows a great deal of evidence for extensive deposition of materials. *Malin and Edgett* [2000] describe sedimentary layers observed in Mars Orbiter Camera images in many different places across the planetary surface, some as thick as 4 km. *Tanaka* [2000] also proposes that thick (hundreds to thousands of meters) dusty and/or icy deposits accumulated in various places on Mars in the Noachian and Early Hesperian. *Kreslavsky and Head* [2000] found that terrain at high latitudes (poleward of $\sim$30°S in Noachis Terra) has less roughness at a horizontal scale of 600 m than equatorial terrain, and their modeling suggests that sediments averaging a few meters in depth could account for this smoothing. Some sedimentary materials are known to be sources for some dune fields on Mars: *Byrne and Murray* [2002] and *Edgett et al.* [2003] found two thick layers of sediments comprising the northern Martian polar layered terrain, the lower of which is the sand source for the extensive northern polar ergs. It appears that an enormous amount of fine-grained material has accumulated over Mars' history, and that erosion of this material and its subsequent redeposition (probably driven by climate changes) is a dominant geological process acting on the Martian surface.

[8] Mafic sand-sized grains on Mars may be produced by volcanic, water, aeolian, glacial, or impact processes. It is unclear which of these processes have dominated the dune sand supply, but with further investigation the relative importance of these processes may be determined. Volcanic eruptions can produce mafic materials that either originate as sand-sized particles or can be eroded down to this size [*Edgett and Lancaster*, 1993]. Water can break rocks into sand-sized grains, along both shorelines and river channels (this process dominates on Earth). The Martian wind can abrade easily erodible rocks [*Bridges et al.*, 2003]. Dunes often form from terrestrial glacier outwash [e.g., *Livingstone and Warren*, 1996], and it is unclear what role Martian glaciers may have had in producing dune sand. Impact gardening is predicted to produce a great amount of sand-sized material [*Hartmann et al.*, 2001] which might contribute to dunes. Such processes may produce a concentration of sand-sized grains, which then may (or may not) be redistributed by other geological processes into materials that become source regions for sand transport pathways and dune fields. The volume, areal extent, exposure, and erodibility (the sediment supply, in the terminology of *Kocurek and Lancaster* [1999]) of these materials partly determines the size and activity of sand transport pathways and dune fields.

[9] Martian sand sinks, places where sand comes to rest, are similar to those on Earth, but with a few exceptions. On the Earth a major sink for sand and dust is water: a great amount of sediment accumulates on the floors of oceans and lakes, and rivers often block the transport of sand across them. If this was once true for Mars, it is certainly not the case in the present cold and dry climate. Topographic obstacles impede sand transport on both Earth and Mars, as does the presence of sand sheets and dunes which absorb kinetic energy from saltating grains [*Bagnold*, 1941]. Vegetation on terrestrial dunes can anchor the edges of barchan and transverse dunes, allowing them to flip in orientation and turn into parabolic dunes [*McKee*, 1979]; obviously, this process is not observed on Mars. Snow and ice can effectively freeze dunes during the winter in high latitude dune fields on Earth [e.g., *Calkin and Rutford*, 1974]. Similarly, the seasonal ice caps likely play a role in stabilizing dunes on Mars. Generally, the sand sinks on Earth have a greater variety than the known sand sinks on Mars. Ideally, this makes interpretations of the local wind regime simpler, because fewer processes need to be taken into account.

[10] The present-day wind circulation pattern is consistent with most, but not all, wind-related features on the Martian surface [*Greeley et al.*, 1993, 1999; *Fenton and Richardson*, 2001; *Bridges et al.*, 1999]. Grain-moving wind activity has been observed in Meridiani over the duration of the Mars Exploration Rover (MER) mission [*Sullivan et al.*, 2005], indicating that at least some amount of aeolian activity is occurring in the present epoch. Over the past several million years, orbital oscillations on a timescale of $\sim 10^5$ Martian years have made the obliquity range from 15°–45°, the orbital eccentricity vary from 0–0.11, and the argument of

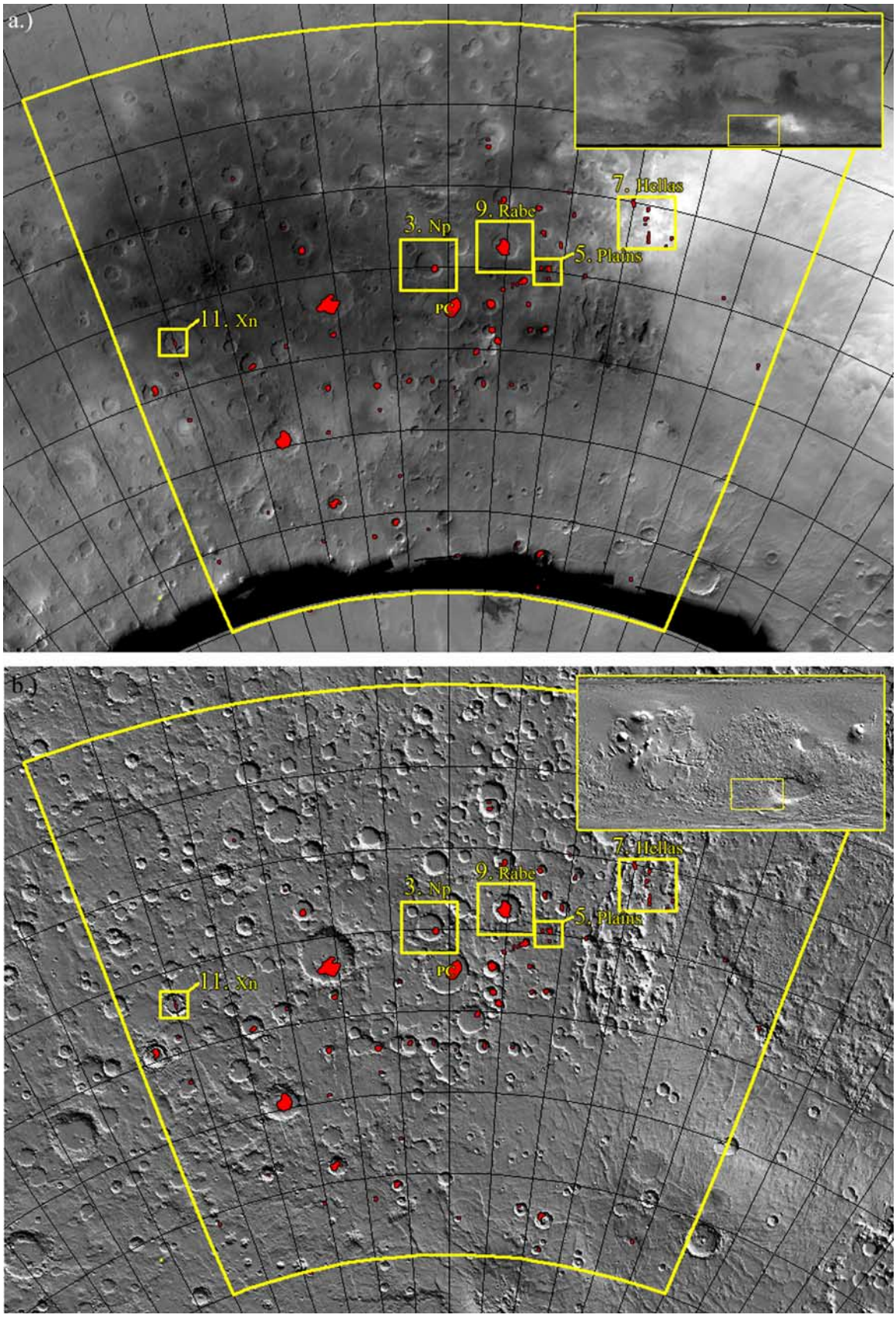
a.)
7. Hellas
9. Rabe
3. Np
5. Plains
PC
11. Xn
b.)
7. Hellas
9. Rabe
3. Np
5. Plains
PC
11. Xn

Figure 1

perihelion precess through the Martian orbit [*Ward*, 1992]. Using general circulation models to study how these factors influence wind circulation, different orbital states are predicted to influence wind strength [*Haberle et al.*, 2003] but not wind directions [*Fenton and Richardson*, 2001]. Thus wind activity varies with the global climate, possibly forcing aeolian features (such as dunes and sand transport pathways) to stabilize or reactivate based on the wind energy, especially during times of high obliquity.

1.3. Study Area

[11] The study area chosen for this work is the Noachis Quadrangle (MC-27) in the southern highlands of Mars. It extends from 0–60°E and 30–65°S. The eastern quarter of the quadrangle is dominated by Hellas Planitia and the surrounding Hellespontus Montes that comprise the rim of Hellas. The remainder of the terrain consists of large, eroded craters, many of which have intracrater dune fields.

[12] The MC-27 quadrangle is shown in Figure 1, both on a MOC wide-angle mosaic (Figure 1a) and on a MOLA shaded relief map (Figure 1b). Red areas with black outlines indicate places where dark dune fields are visible in either MOC narrow-angle or THEMIS VIS images. The dune fields appear in a broad northeast-southwest trending swath across the quadrangle. Yellow boxes indicate the locations of other figures in this work.

[13] In the years before the Mars Global Surveyor mission, the intracrater dune fields of the southern mid and high latitudes and the northern polar ergs were thought to be the most significant accumulations of sand on the planet [*Greeley et al.*, 1992]. Indeed, it was in the Noachis Quadrangle that dunes were first identified in Mariner 9 images [*Cutts and Smith*, 1973]. The large dune fields in this region, particularly those in Proctor and Rabe Craters, have since been targets of a number of studies. Comparisons of these dunes with terrestrial dunes showed that dune widths and spacing were similar on both planets [*Breed*, 1977; *Breed et al.* 1979]. Morphological studies led to the classification of these dunes as crescentic [*Ward et al.*, 1985] or dunes with multiple slipfaces [*Lancaster and Greeley*, 1987]. The surrounding intercrater plains have also been of interest in aeolian research for the bright and dark wind streaks that have formed form (and some of which shift or reform over time) in the lee of topographic obstacles [e.g., *Thomas and Veverka*, 1979; *Thomas et al.*, 1984].

[14] Data from more recent spacecraft missions have allowed for further analysis of aeolian processes in Noachis Terra. For example, *Edgett and Malin* [2000a] show MOC narrow-angle images of linear features on dune slipfaces in both Proctor and Rabe Craters, arguing that these features are evidence for recent dune activity. *Fenton et al.* [2005] focused on the dunes in Proctor Crater, concluding that they displayed as many as three different slipface orientations, which were interpreted as three formative wind directions. Although *Fenton et al.* [2005] mention the lack of an obvious sand transport pathway near the Proctor Crater dunes, to date, no study in this area has concentrated on seeking out and interpreting sand transport pathways.

1.4. Three Categories of Sand Sources

[15] Sand sources can be (somewhat arbitrarily) grouped into three different categories based on their size and distance from the dune fields: "distant," "local," and "regional." Sand derived from a "distant" source comes from an upwind location that may feed into one or more dune fields that may be far (i.e., located more than several mean dune field widths) from the source. For example, most of the sand in the Kelso Dune complex (with a mean dune field width of ~13.2 km) can be traced upwind ~55 km to a distant source: alluvial sediments from the Mojave River [*Sharp*, 1966]. On Mars, potential "distant" sand sources might be volcanic ash or outflow deposits that are exposed to wind erosion, which then may carry this material across many (perhaps hundreds of) kilometers before it accumulates as dunes. "Local" sources of sand come from one or more nearby (i.e., located within one mean dune field width) discrete areas that collectively feed sand into a nearby dune field. For example, minor amounts of sand in the Kelso Dunes are derived from washes carrying material down from neighboring mountains [*Ramsey et al.*, 1999]. On Mars, a potential local sand source might be gullies in crater walls, which may transport sand a few kilometers to the crater floor. "Regional" sources are widespread areas (i.e., from an area more than several times the dune field area) from which sand may erode, contributing to one or more nearby dune fields. "Regional" sources may be located some distance from, or very close to (perhaps even underlying), a dune field. Terrestrial regional sources may include layers of sandstone or glacial till exposed to erosion over a wide area. For example, a yardang field, such as that in the Taklimakan desert of China, is a potential regional source for the dunes located immediately downwind [*McCauley et al.*, 1977]. Potential Martian analogues may include any available material easily eroded by the wind: yardang fields, crater ejecta, volcanic ash, lacustrine deposits, polar layered deposits, and even ancient indurated dune fields (i.e., the sandstones proposed by *Edgett and Malin* [2000b]). Many dune fields may be formed from sand derived from a combination of these types of sources (e.g., the Kelso Dunes are a combination of Mojave River sediments and sands from nearby washes). Other combination scenarios are possible. A layer of sandstone (regional) may only outcrop in a few places where mountain streams (local) can erode it and thus expose sand to wind erosion,

Figure 1. The Noachis Quadrangle (MC-27), the study area in this work. Both frames were created from JMARS. (a) The MOC wide-angle mosaic at 256 pix. per degree shows most of the quadrangle, but an unsampled strip near the southern edge (~63°–65°S) appears black. (b) The MOLA shaded relief map at 64 pix. per degree clearly shows the ancient cratered terrain that dominates most of the quadrangle. Red polygons outlined in black indicate dunes observed in MOC narrow-angle and THEMIS VIS images. Yellow boxes indicate regions of interest discussed in the following text. Insets in the upper right corner show the location of MC-27 on Mars. The location of Proctor Crater is labeled as "PC."

leading to local derivation of a regional (but buried) source. On Mars, dunes might form from underlying volcanic ash deposits (local or regional), but also incorporate sandblown in from a distant upwind source (distant), producing dunes composed of a mixture of distant and local and/or regional sands.

2. Method

2.1. Data Sets and GIS Applications

[16] Two different Geographical Information Systems (GIS) were used to view the different data sets: JMARS and ArcView. Each application has its advantages and disadvantages, as outlined below, necessitating the use of both systems. Table 1 lists the data set, image identification number, and application used to create each figure discussed in this work. In addition, volume measurements were made using a 128 pixel per degree MOLA DEM with the IDL routine GRIDVIEW [*Roark et al.*, 2000; *Roark and Frey*, 2001]. Volume calculations involve defining the areal extent of a feature as well as four upper and lower bounding elevations; both volumes and cavities may be calculated.

2.1.1. JMARS

[17] JMARS is a Java-based package that provides a layered system with immediate access to several spacecraft data sets of Mars [*Gorelick et al.*, 2003]. An advantage of using JMARS is that it is easy and quick to use, with all images preprojected and prestretched upon rendering. This makes assembly of several tens (or more) of images very efficient. However, the details of individual images may be washed out by the prestretching, and the highest resolution images (in this case, the MOC NA images) are resampled for quick assembly, reducing their quality. In this work, JMARS provides the low resolution mosaics, such as MOC WA mosaics and THEMIS daytime and nighttime infrared (12.57 μm band) mosaics. All figures made from JMARS are in an oblique equirectangular projection; all figures made from ArcView are in a sinusoidal projection, so features in some figures may not line up perfectly from one GIS to another. In this work, the THEMIS instrument name is often dropped: "daytime infrared (IR)," "nighttime IR," and "VIS" images all refer to data products from THEMIS.

[18] In all cases, individual images in JMARS are manually stretched in intensity to best approximate the stretch of the surrounding images. For example, a daytime infrared THEMIS image is stretched to appear similar to surrounding daytime infrared THEMIS images. This process allows surface features that are larger than a single image width (such as a 100 km diameter crater) to be identified with ease. This method has no quantitative value; for example, neighboring THEMIS infrared images from different seasons will not reflect similar temperatures (e.g., summertime images are warmer than wintertime images). However, the stretching is of qualitative use; surfaces that have a high thermal inertia will retain heat at night relative to low thermal inertia surfaces regardless of the season, and surfaces with a low albedo will heat up more during the day than surfaces with a high albedo regardless of the season (assuming wintertime frost cover does not interfere). Because this qualitative analysis appears to be so useful, no attempt is made to quantify albedo and thermal inertia in this work. Rather, qualitative correlations in the different data sets are noted and interpreted.

2.1.2. ArcView

[19] ArcView GIS Version 3.3, created by ESRI (Environmental Systems Research Institute), was used for high resolution detail and topographic maps in this work. ArcView has the advantage of allowing the high resolution MOC NA images ($\geq$1.5 m/pixel) to be displayed at full resolution, with stretching options available for use on each image independently. In addition, a MOLA DEM created with GMT is of a higher resolution than that available in JMARS, and it has been colorized to represent both surface texture and elevation. In this work, ArcView was used for morphological analysis of the MOC NA images and topography.

2.2. Limitations of Visible Images

[20] In this work, observations of dune morphology are made with MOC NA images only. Other visible imagery (such as THEMIS VIS and MOC WA) generally does not provide the details necessary to identify dune slipfaces and other features necessary to analyze the dune fields on Mars (however they can be used to identify the locations of dune fields). The MOC NA images do not cover all of the Martian surface, but most of the dune fields in Noachis Terra are well covered by this instrument, allowing for a detailed analysis.

[21] One caveat of visible imagery is that observations are dependent on lighting angle and season. When the sun is low in this sky, topography becomes enhanced; when the sun is high in the sky, albedo is enhanced. On Mars, the large dunes are almost always dark relative to the surrounding terrain, making their presence more easily detectable in summertime images. However, slipfaces are more clearly seen in wintertime images, when the sun is lower in the sky and the shading of steep slopes makes stoss and slipface identification easier. Of more concern is locating nearby sand sheets and drifts of sand in small pockets. Figure 2 shows a typical example of a region with partial dark sand cover. In the winter (Figure 2a) most of the brightness variation is caused by topography: for example, both the small ripple-like bedforms in the upper right and the layered slopes leading to flat mesa tops in the left and bottom of the frame are quite apparent. In the summertime image (Figure 2b) most of the brightness variation is caused by albedo differences. The texture of the mesas and layers is barely visible, and the ripple-like bedforms stand out because they are brighter than the underlying terrain, rather than from their height or slopes. A dark patch interpreted here as dark sand is apparent in the summertime image; it would be very difficult to identify in the wintertime image. MOC NA coverage is generally sparse, and overlapping images such as the two shown in Figure 2 are rare. Thus identification of sand transport pathways in MOC NA images is dependent on both MOC NA coverage and the season at which they were obtained.

2.3. Outlines of Dune Fields in Mosaics

[22] In the following figures, red outlines indicate the location of dunes and isolated dark sand drifts far from dune fields identified in both MOC NA and THEMIS VIS images. In many cases, dark surfaces suggestive of dune fields are visible in MOC WA images, but the resolution of the MOC WA mosaics ($\sim$230 m/pixel) generally does not

Table 1. Images and GIS Applications for Each Figure

Figure	GIS	MOC NA	THEMIS VIS	Daytime THEMIS IR	Nighttime THEMIS IR
1	JMARS	N/A	N/A	N/A	N/A
2	ArcView	E02/00791 E14/00275	N/A	N/A	N/A
3a, 3b, 3c	JMARS	R09/03986 M09/01743 M02/01511 E02/00791 R08/02177 E03/00313 M03/06829 E09/01078 M00/01650 E11/02545 M02/00203 E14/00275 M08/08032 R14/02423	N/A	I06441006 I06703002 I07165004 I09786004 I09549003 I02234002 I01897002 I01485002 I08226002 I07839003	I09680013 I01329005 I07683009 I07246010 I06934003 I00967002 I10616002 I01304006 I08744005 I11452002 I08020010 I05486003 I10591002 I06235008 I11215002
3d	ArcView	N/A	N/A	N/A	N/A
4	ArcView	M03/06829 M08/08032 E09/01078	N/A	N/A	N/A
5a, 5b, 5c	JMARS	E14/01531 E10/00456 E12/00457 E16/00358 E02/00064	N/A	I09898004 I09636004 I09611006 I06503002	I08132009 I05598006 I08519013 I08544011 I06996008 I08831010 I06322008 I06272004
5d	ArcView	N/A	N/A	N/A	N/A
6	ArcView	E10/00456 E12/00457	N/A	N/A	N/A
7a, 7b, 7c	JMARS	R11/01487 M15/01028 R11/04554 M11/00400 M13/00104 M13/01617 E18/00031 E16/00153 M21/00514	V10347004 V10422002 V10397004 V10372001 V08887001 V08862013	I05991004 I07414003 I08500003 I07102002 I08163004 I07077003 I08138004 I07052005 I07826004 I07027002 I07801005 I07002003 I07776009 I07726005 I07751004 I08088006 I07489002 I06253002 I07439003	I08681008 I06459009 I07932008 I06384015 I09904015 I06022005 I09567012 I05685008 I09542006 I05635008 I07957011 I05373002 I11464002 I05348005 I10478008 I05323002 I06746005 I05298002 I06484015
7d	ArcView	N/A	N/A	N/A	N/A
8	ArcView	E18/00031 R11/01487	N/A	N/A	N/A
9a, 9b, 9c	JMARS	R14/01181 E11/00389	N/A	I02496002 I08513003 I02471002 I08126004 I01747003 I08076004 I01410002 I08051005 I09661003 I08026005 I09424004 I06166002 I09037002 I05055002	I07845010 I08544011 I07920011 I08182008 I08232010 I07870010 I01179002 I07096010 I06784005 I06322008 I09555013 I05598006 I09867008 I08207009 I09530014 I10154003
9d	ArcView	N/A	N/A	N/A	N/A
10a, 10b	ArcView	M02/03078 E14/01895 M03/03547 R11/03716 E02/00691 R14/-01181 E04/01339 R15/00353 E11/00389 R15/02482	V02496003	N/A	N/A
10c	ArcView	E11/00389 R14/01181	N/A	N/A	N/A
10d	ArcView	R11/03716	N/A	N/A	N/A
10e	ArcView	R15/00353	N/A	N/A	N/A
11a, 11b, 11c	JMARS	E10/01271	N/A	I01773002 I08052008 I01748004 I03221002 I09425003 I03196002 I10361005	I07871010 I05287002 I07921012 I01255004 I07509006 I01230002 I10467007 I02316006
11d	ArcView	N/A	N/A	N/A	N/A
12	ArcView	E10/01271	N/A	N/A	N/A

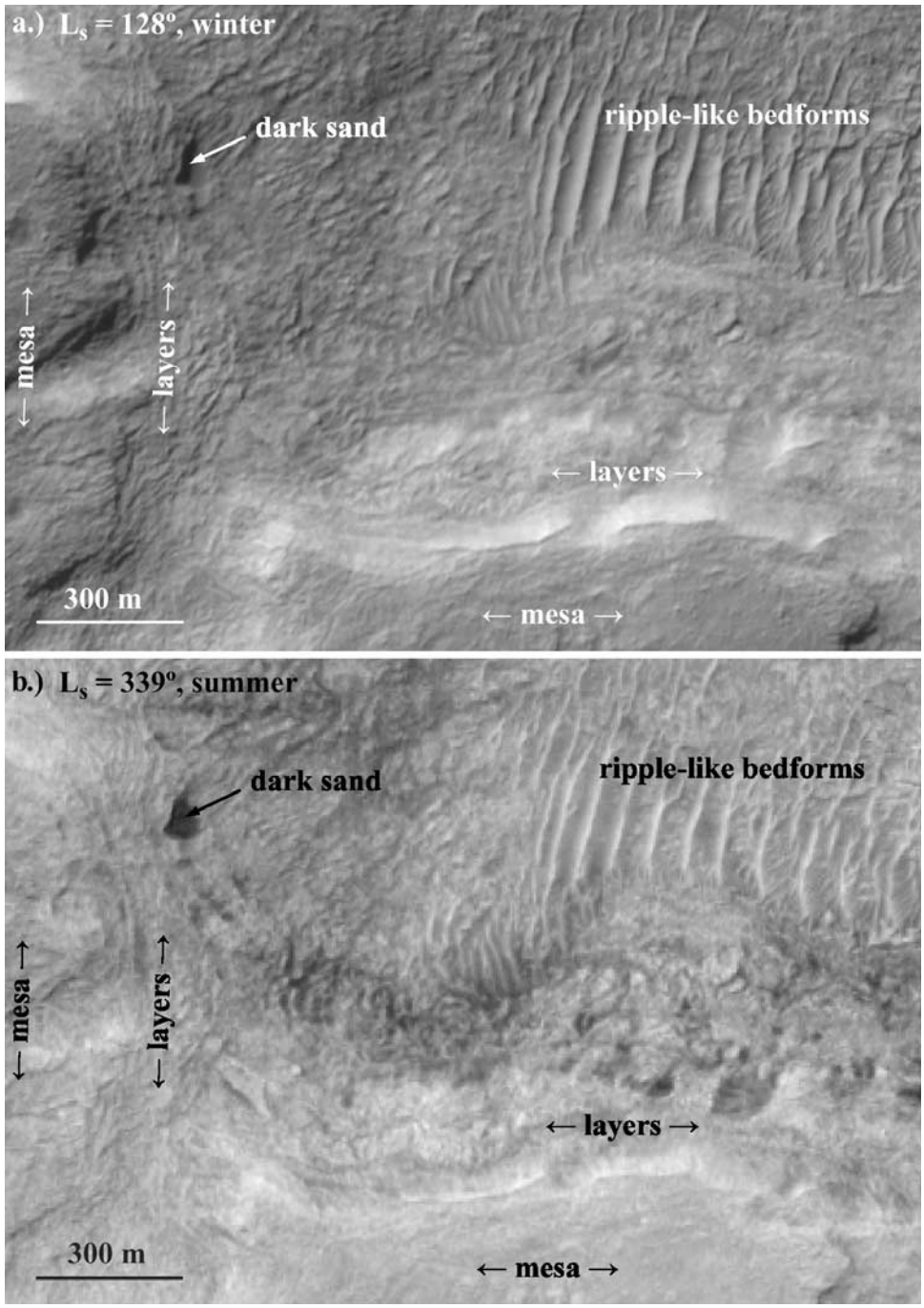

Figure 2. Portions of MOC narrow-angle images (a) E02/00791 and (b) E14/00275, showing winter and summer images (respectively) of the same area within the larger pit in crater Np. Topography is easy to discern in the winter image, but the sand accumulations are difficult to spot. In the summer image, sand accumulations are easier to identify, but topography such as layers on mesa walls is more difficult to spot. The generally poor coverage and seasonal variability of visible imagery at this resolution lead to many difficulties in image interpretation.

resolve individual dunes, and it is easy to confuse dark dunes with dark sand sheets or other dark surfaces. Therefore the red outlines indicate positively identified dunes or accumulations of dark sand.

2.4. Dune Slipfaces and Rose Diagrams

[23] Dune slipfaces are produced by a combination of grainfall and grainflow. Grainfall occurs when grains are lifted into saltation and/or suspension and carried across the brink of a dune, falling out onto the lee side. As the sand deposited by grainfall accumulates, it produces a bulge of sand near the brink that eventually oversteepens and avalanches in a process called grainflow [e.g., *McDonald and Anderson*, 1995; *Nickling et al.*, 2002]. It is grainflow that is thought to control a dune's migration. Continued avalanching produces the characteristic slipfaces that are used both

to identify dunes and to determine the direction of the wind that influences the dune; slipfaces are always oriented transverse to the wind (i.e., they dip downwind).

[24] Because of this, dune slipfaces that are visible in spacecraft images provide information about certain aspects of the wind regime present while the dunes are (were) active. Sand saltates only when the stress exerted by the wind upon the surface exceeds a threshold value. Furthermore, rather than being linearly related to the wind strength, sand flux is proportional to the cube of the shear velocity,

$$q \propto u_*^3, \tag{1}$$

where q is mass flux in mass per unit width per unit time and u_* is shear velocity, related to the wind velocity u as a function of height z by the Prandtl-von Karman equation:

$$u(z) \propto u_* \ln(z). \tag{2}$$

(For further information, see discussions by *Bagnold* [1941] and *White* [1979].) Because the strongest winds move the most sand, it is these winds that dominate dune morphology. Thus winds below the saltation stress threshold, no matter how often they blow, are not reflected in dune morphology. Rather, dune slipfaces are produced by persistent winds that blow above the saltation threshold, especially by very strong winds. For example, it is possible for terrestrial dunes to remain inactive throughout the year, only to move several meters downwind in a sudden wind storm.

[25] Using a rose diagram (i.e., polar histogram), conclusions may be drawn about the wind regime in which the Noachis Terra dunes form, as well as how the wind regime varies from one dune field to another. Comparisons of terrestrial dune morphology with wind measurements by *Fryberger* [1979] have led to the following generalizations. Barchans, barchanoid dunes, and transverse dunes generally form in a directionally uniform wind regime, leading to a unimodal wind distribution on a rose diagram. Linear dunes are produced by two distinct winds of roughly the same magnitude (each wind is usually associated with a particular season), producing a bimodal rose diagram. Star dunes are produced by three or more sand-moving winds, producing a multimodal rose diagram. Although *Fryberger* [1979] obtained wind information from direct wind measurements, no direct wind measurements are available of this region on Mars. In this work, dune slipface orientations are used as a proxy for wind measurements, and it should be noted that the resulting rose diagrams are biased toward the strongest prevailing winds above the saltation threshold.

[26] Slipfaces were identified in the MOC NA images of three different dune fields discussed below in order to estimate their orientations, thereby inferring dune-forming wind orientations. Barchans and barchanoid dunes have crescentic slipfaces and transverse dunes have long steep slipfaces that reach from the dune brink to the ground. Following the method used by *Fenton et al.* [2005], the downwind direction of each feature is estimated by hand. Only the clearest cases are considered slipfaces; these are typically dunes near the edge of the dune fields where sand supply limits dune morphology and more classical barchan and transverse dunes are visible. Although some dunes in the centers of the dune fields resemble linear or star dunes, it is often difficult to determine from inspection whether a given slope is a slipface or a stoss. It is possible that some complexities of the wind regime may be overlooked by omitting slipfaces in the central parts of the dune fields, but the slipface orientations represented by the smaller dunes at the edge of the dune field tend to compare well (qualitatively) with those represented by the larger, more intricate dunes. For each dune field measured, a rose diagram is created of the dune slipface orientations (in the downwind direction). The rose diagrams show orientations binned in 10° intervals. The resulting rose diagram represents the wind regime for the strongest and most frequent winds acting upon the dunes.

2.5. Assumptions About Sand

[27] In this work, the assumption is made that all of the sand in Noachis Terra consists of low albedo lithic fragments of roughly the same particle diameter, and that have a mafic composition. Thus the sand discussed in this work appears dark in the MOC WA mosaics and bright in the daytime infrared mosaics. At night, the sand is assumed to have a signature cooler (darker) than that of solid rock and brighter (warmer) than that of loose dust. Areas that fit all of these descriptions, even where there are no high resolution MOC NA images to verify the presence of sand or dunes from a morphological perspective, are generally assumed to be sand.

[28] *Fenton et al.* [2003] performed a spectral deconvolution of Thermal Emission Spectrometer (TES) data on the Proctor Crater dune sand and found a composition consistent with basaltic sand. They also found TES thermal inertias of the dune field indicative of coarse sand (740 ± 170 μm), a result similar to that of many other researchers.

[29] The actual situation in Noachis Terra may be far more complicated. For example, there may be relatively bright sand present as sand sheets that cannot be distinguished from other mantling materials. The thermal and/or compositional properties of the dark sand may vary from dune field to dune field, biasing the interpretations of the data. *Aben* [2003] shows that spectral deconvolution of TES data indicates that although many dune fields in Noachis Terra are consistent with basaltic sand, some dune fields indicate the presence of some amount of sand with an infrared spectrum of either andesite or weathered basalt. It may be that as more data becomes available, such refinements can be made and the sedimentary history of Noachis Terra be examined in more detail.

3. Results

[30] Five regions of Noachis Terra containing dune fields have been investigated and are discussed in detail. Although other dune fields in Noachis Terra have been inspected, these regions span the range of terrains that contain dune fields and are considered here to be representative of most of Noachis Terra. The five regions include dune fields inside and outside large pits on crater floors as well as intercrater dune fields. In each case, the terrain and its relation to aeolian features is described in both visible and infrared

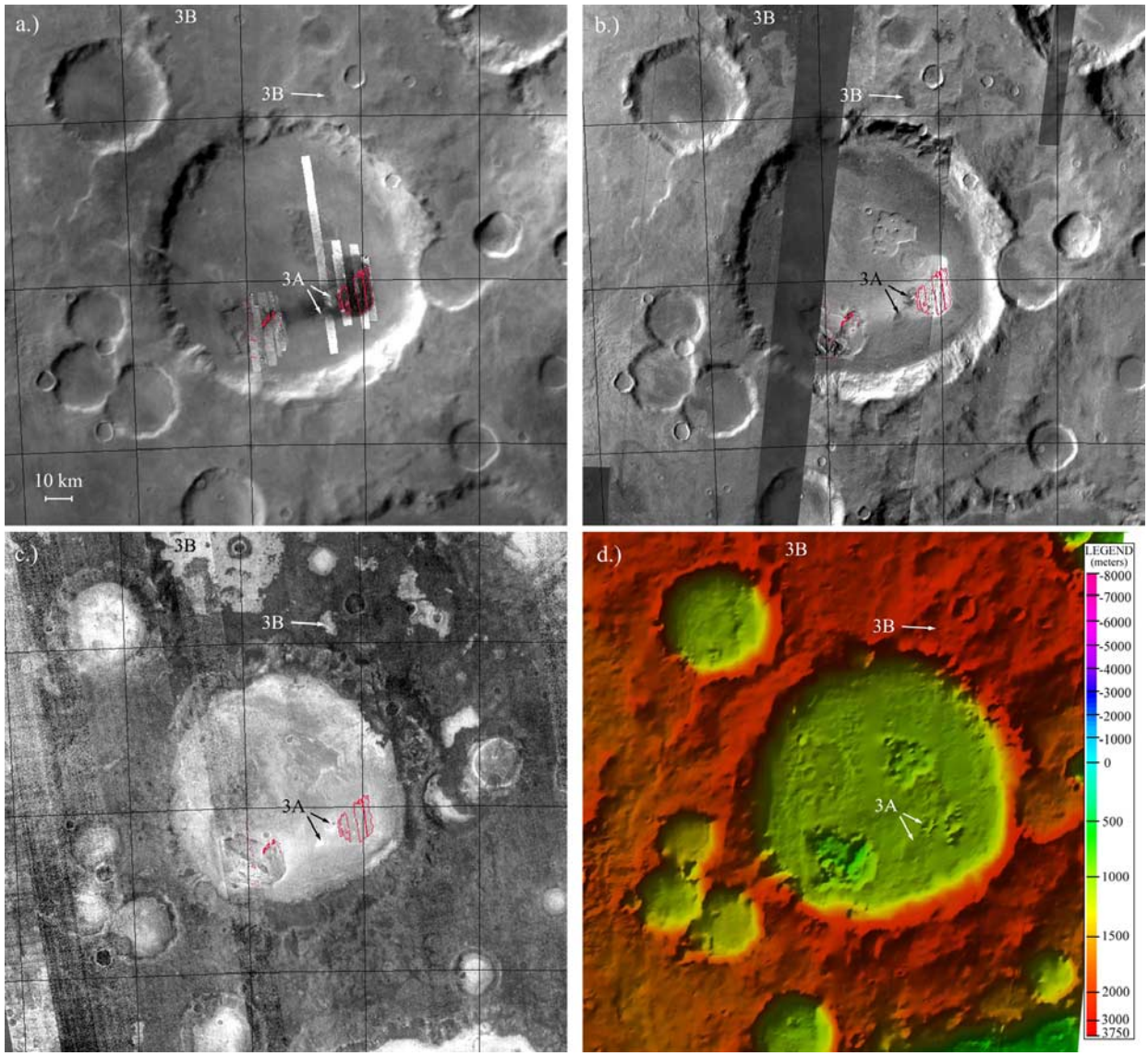

Figure 3. Crater Np, a 100 km diameter crater north of Proctor Crater. A small dune field has accumulated in the southeast corner of the crater, and two pits have eroded into the crater floor. (a) MOC WA mosaic with several MOC NA images superimposed (JMARS), (b) THEMIS daytime IR mosaic (JMARS), (c) THEMIS nighttime IR mosaic (JMARS), and (d) MOLA DEM and shaded relief (ArcView). Dunes in MOC NA images outlined in red. Note 3A just west of the dune field, night-bright (warm) and day-dark (cool) in THEMIS IR; and 3B, patches on the intercrater plains that are night-bright (warm) and day-dark (cool) in THEMIS IR.

mosaics. MOC narrow-angle images illustrating smaller-scale characteristics of the dunes and surrounding terrain are presented. Where dune fields are located near (or within) crater floor pits, the volumes of the pits and dune fields are compared.

3.1. Crater Np

3.1.1. Crater Np: Mosaics

[31] Crater Np (see Figure 3) is a 100 km diameter crater in the middle of Noachis Terra (29°E, 45°S). It is located just north of the larger Proctor Crater (marked as "PC" in Figure 1). Like many of the larger craters in this area, crater Np contains a dune field, although it is one of the smaller intracrater dune fields (12 km × 17 km). In this study, crater Np is intended to represent a typical impact crater containing a dune field. Excellent coverage by THEMIS in both day and night IR images also makes this crater a good candidate for study.

[32] The dunes have accumulated in the southeast part of the crater floor (see Figure 3a). Most of the crater floor is flat but punctured with the occasional impact crater. There are two shallow pits, each covering roughly the same area as the dune field. One is located in the southwest part of the crater floor, and it has a depth of ~300 m below the crater floor. The second pit is located in the central-northeast part of the crater floor, and it has a depth of ~100 m below the

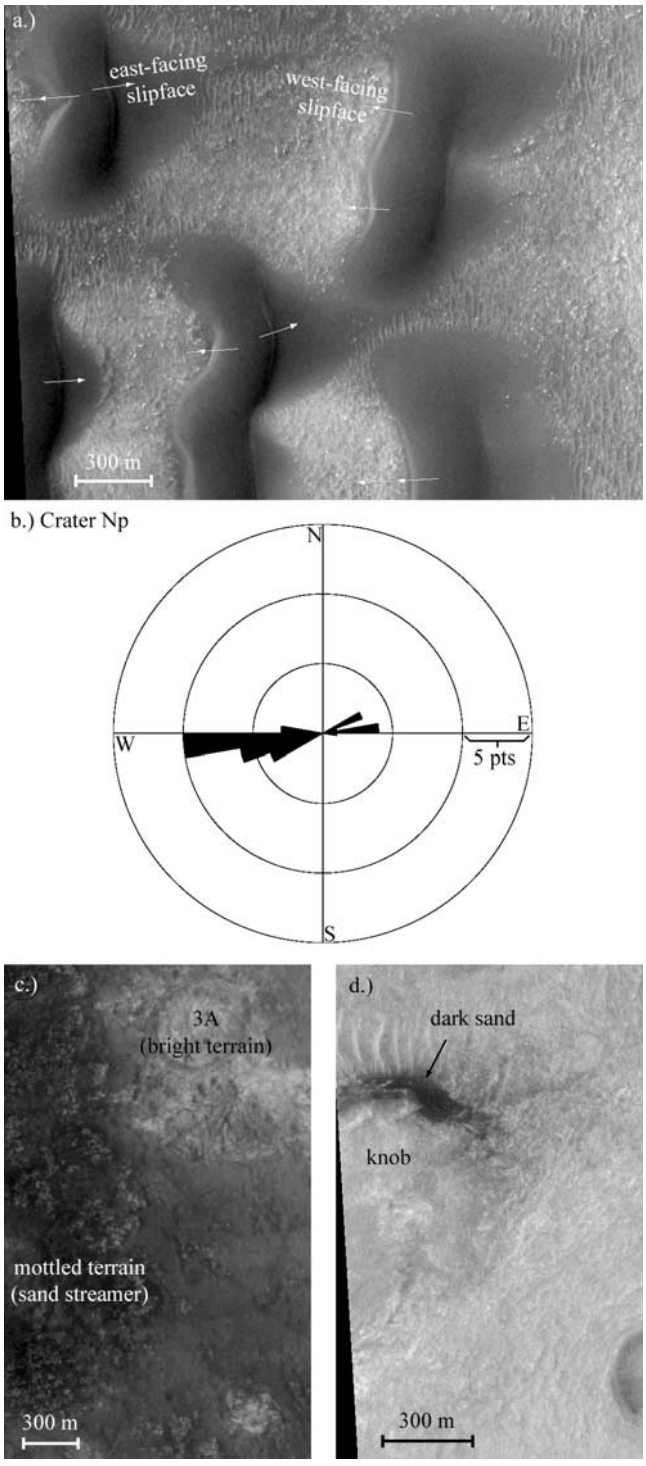

Figure 4. MOC NA images of Crater Np: (a) M03/06829, showing dark dunes and two opposing slipfaces. (b) Rose diagram of crater Np dune slipface orientations (indicating downwind direction). Portions of MOC narrow-angle images (c) E09/01078, showing the dark surface interpreted as a sand sheet and bright terrain that appears to have a high thermal inertia, and (d) M08/08032, showing a dark sand patch on the northeast side of a knob in the southwestern pit in crater Np: is it a falling or a climbing dune?

crater floor. It is not clear what erosional process formed these pits, but they are common on the floors of larger craters in Noachis Terra.

[33] Figure 3a shows MOC NA images of the dune field and southwestern pit superimposed on a MOC WA mosaic. A dark band, interpreted here as a sheet of dark sand, connects the dune field to the southwestern pit. Dunes in the dune field and accumulations of dark sand in the southwestern pit are outlined in red. It is unclear from the scale of Figure 3a whether the dark sand sheet is carrying sand from or into the dune field.

[34] Because of their albedo, the dark dunes appear bright (warm) in daytime IR images (see Figure 3b). The sand sheet appears as a bright region between the dunes and the southwestern pit. However, at night the dark sand is less apparent (see Figure 3c). The dune field appears slightly darker (cooler) than the immediately adjacent terrain, but elsewhere on the crater floor the surface is just as dark, or darker, as that of the dunes. At night, the dark sand sheet is difficult to distinguish from the surrounding crater floor. In fact, the region between the dunes and the southwestern pit is among the brightest areas on the crater floor, contrasting with the slightly darker dunes.

[35] Immediately west of the dune field, there are two ~5 km wide spots that appear bright in the MOC WA mosaic (Figure 3a), contrasting with the surrounding dark sand sheet (labeled "3A" in Figure 3). Their albedo appears to be similar to that of the rest of the crater floor. In the daytime IR mosaic (Figure 3b), these spots appear dark (cool) relative to both the brighter sand sheet and the most of the crater floor. This contrast with respect to the crater floor suggests that the spots are made of a more competent or rough terrain than the rest of the crater floor. This is supported by inspection of the nighttime IR mosaic (Figure 3c), in which the spots appear bright (warm). These spots have no topographic signature in the MOLA DEM (see Figure 3d), giving no hint as to what sort of structures they may be (but see discussion of MOC NA image in section 3.1.2).

[36] On the intercrater plains, the image mosaics indicate strikingly different thermal properties from those on the floors of both crater Np and other surrounding craters. The MOC WA mosaic (Figure 3a) indicates a surface of fairly uniform albedo. The daytime IR mosaic (Figure 3b) shows surface temperatures largely influenced by topography. The typical range of temperatures within a single THEMIS daytime image is on the order of 30 K, changing the most from sunlit to shaded slopes. In contrast, the nighttime IR mosaic (Figure 3d) shows a great deal of temperature variation that is unrelated to topography. The typical range of temperatures within a single THEMIS nighttime image of roughly the same season is on the order of 20 K, varying the most from crater floors to the intercrater plains. In the nighttime IR mosaic, most of the crater floors are bright (warm), although the floors of the smallest (<~8 km) craters are dark (cool). In contrast, most of the intercrater plains are relatively dark (cool) at night. The few areas on the intercrater plains that are bright (warm) at night (labeled "3B" in Figure 3) are slightly darker (cooler) in the daytime IR and barely appear as faint, slightly darker patches in the MOC WA mosaic. These night-bright areas show the same thermal characteristics as the two small spots on the floor of crater Np (labeled "3A"). It is unclear at this scale what

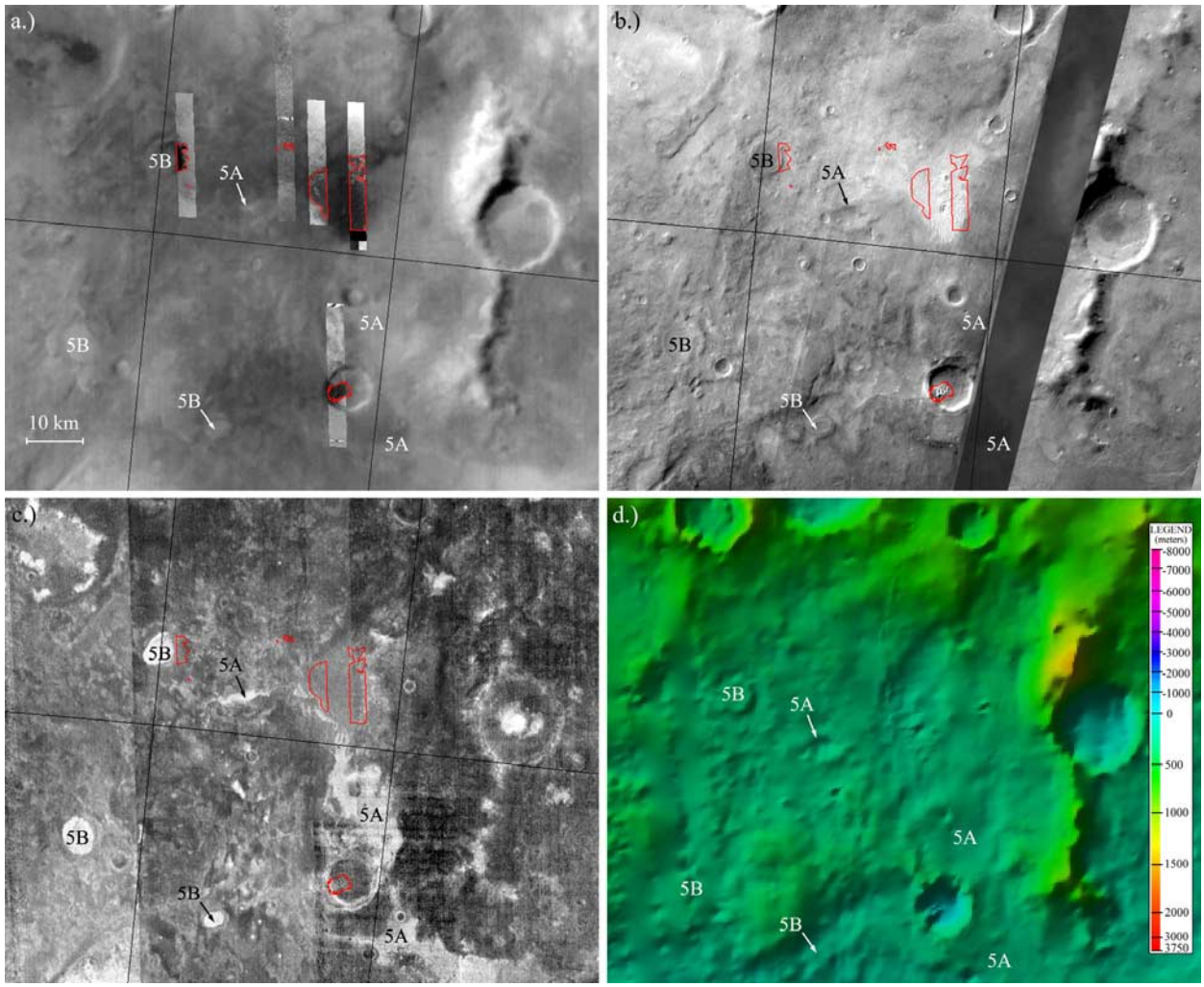

Figure 5. Dune field on the intercrater plains: most in Noachis Terra are located in craters, but this one is set in a local topographic low out on the intercrater plains. (a) MOC WA mosaic with five MOC NA images superimposed (JMARS), (b) THEMIS daytime IR mosaic (JMARS), (c) THEMIS nighttime IR mosaic (JMARS), and (d) MOLA DEM and shaded relief (ArcView). Dunes in MOC narrow-angle images outlined in red. Note IR night-bright (warm) patches 5A and 5B and their lack of signature in both MOC WA and daytime IR mosaics.

these night-bright areas are and how areas 3A and 3B may or may not be related.

3.1.2. Crater Np: MOC Narrow-Angle Images

[37] MOC NA images reveal the morphology and characteristics of many of the features that are barely distinguishable in the lower resolution mosaics. For example, the dunes in crater Np appear to be transverse ridges separated by higher albedo interdunes (see Figure 4a). Most slipfaces are oriented roughly westward (left-pointing arrows in Figure 4a). However, close inspection shows that some of the dunes have slopes on their opposing sides. These slopes are interpreted here as roughly eastward-oriented slipfaces (right-pointing arrows in Figure 4a). This morphology is unlike anything observed on terrestrial dunes, in which opposing slipfaces in reversing or linear dunes meet at a peak at the crest of the dune [e.g., *McKee*, 1979]. These separated slipfaces have also been observed in the dunes within Proctor Crater, located roughly 150 km to the southeast of crater Np.

[38] Measurements of slipface orientations were made where possible in each of the MOC NA images of the dune field in crater Np. Several examples of such measurements are shown as white arrows in Figure 4a. The orientations of all measured slipfaces are shown as a rose diagram in Figure 4b. Because these dunes are inferred to be transverse, these slipfaces are interpreted to indicate the downwind direction of the dune-shaping winds. In the dune field, most slipfaces are oriented toward the west-southwest, indicating dominant winds blowing from the east-northeast. However, a few slipfaces are oriented toward the east-northeast, indicating secondary winds blowing from the west-southwest.

[39] MOC narrow-angle images also provide detail of features on the floor of crater Np. Figure 4c shows an area on the floor of crater Np just west of the dune field. The brighter area, labeled "3A" corresponds to the area (also labeled "3A" in Figure 3) that also appears bright in the MOC WA mosaic (indicating high albedo relative to the

surrounding terrain), bright in the nighttime IR mosaic (suggesting a higher thermal inertia or rougher terrain relative to the surrounding terrain), and dark in the daytime IR mosaic (consistent with both a higher relative albedo and higher relative thermal inertia or rougher terrain). In Figure 4c, this bright area lies adjacent to a darker, mottled surface that is interpreted in this work as a sand sheet. The mottled nature of this darker surface may indicate a rougher, perhaps blocky, surface that traps dark sand. The brighter spots within the mottled surface may be boulders or erosional remnants that poke through the dark sand cover. The smoother nature of the adjacent bright terrain (3A) suggests that the thermal signature at night is more consistent with a high thermal inertia material than a highly textured terrain, both of which can contribute to high nighttime surface temperatures.

[40] It is not clear from Figure 3d or 4c if the bright terrain (3A) stands out topographically. Sand tends to accumulate in topographic lows; the fact that dark sand appears to be present in areas surrounding, but not on, the bright terrain (3A) suggests that the bright terrain itself is a positive topographic feature. However, the smoother apparent texture of this bright terrain could also prevent dark sand from accumulating there, leaving its relative topographic signature ambiguous.

[41] Figure 4d shows an area in the floor of the southwestern pit containing an accumulation of dark sand. The sand has piled up on the northeast side of a ~600 m wide knob. Measurements of dune slipfaces indicate two possible sand-moving winds in crater Np: one from the east-northeast and one from the west-southwest (see Figure 4b). In terrestrial deserts, sand accumulates on both the upwind and the downwind sides of topographic obstacles (e.g., climbing and falling dunes of *Livingstone and Warren* [1996]). Without any discriminating features, it is difficult to determine whether this sand accumulated on the downwind side of the knob (as a falling dune), blown by winds from the west-southwest, or on the upwind side of the knob (as a climbing dune), blown by winds from the east-northeast. Thus the directional ambiguity of the dark sand sheet between the southwest pit and the dune field in crater Np remains unresolved.

3.1.3. Crater Np: Volumes

[42] One unresolved question is whether the dune sand in crater Np could have been supplied by material eroding from the southwestern pit. If the volume of dune sand is greater than that of the southwestern pit, then the pit could not be the sole source of dune sand. However, if the volume of dune sand is less than that of the southwestern pit, then the pit cannot be ruled out as the sole source of dune sand.

[43] Using the IDL routine GRIDVIEW, the cavity volume of the southwestern pit was found to be ~47 km^3. The volume of the dune field was found to be ~7 km^3. Because the MOLA spot size has a similar areal extent as the dunes themselves (130 m wide with an along-track spacing of 330 m), the dunes are not well sampled and the volume calculation may be underestimated (i.e., the dunes are aliased). Even if the dune field volume is underestimated by a factor of 2–3×, the dune field is smaller than the southwestern pit. Thus it is possible that the dune sand may be derived entirely from eroded pit material.

3.2. Dunes on the Intercrater Plains

3.2.1. Intercrater Plains: Mosaics

[44] Although most dunes in Noachis Terra are located in craters, there are a few exceptions. One of these is a dunefield out on the intercrater plains at 38.5°E, 45°S, located east of Proctor Crater, southeast of Rabe Crater, and ~40 km west of the edge of the Hellas Basin (see Figure 5). Wind conditions, sand supply, and surface roughness are all characteristics that may vary between the crater floors and the intercrater plains, leading to the question of how those varying parameters influence dune morphology and sand transport paths.

[45] Figure 5a shows a MOC WA mosaic superimposed by five MOC NA images of dunes. Dunes visible in MOC NA images are outlined in red. There are a number of areas with dune fields. In the middle is the largest (here called the main dune field), roughly 8 km × 14 km. To the west of the main dune field are several individual dunes (the smallest red outlines) and one ~5 km × ~2 km dune field that appears to have formed on the eastern wall of a round mesa. South of the main dune field is a ~3 km × ~4 km dune field on the west side of a small 9 km diameter crater. In the northwest corner of Figure 5a is a dark patch that looks suspiciously like a dune field, but no THEMIS VIS or MOC NA images cover that area, so their identification as dunes (as opposed to a sand sheet or dark bedrock) must remain until more data is available.

[46] Figure 5b shows a daytime THEMIS IR mosaic of the intercrater plains area. Except where shaded, all of the dunes appear bright (warm), absorbing solar energy as a result of having a low albedo and heating up during the day. In both the MOC WA mosaic and the daytime IR mosaic, visibly dark and daytime thermally bright material extends at least halfway between the main dune field and the western dunes outlined in red. This material is interpreted here as a dark sand sheet, similar to that found in crater Np (see Figures 3a and 3b). It is likely that further MOC coverage will reveal more individual dunes in this sandy area. In the nighttime IR mosaic (Figure 5c), the dunes appear intermediate in temperature relative to the surrounding terrain. As with the sand sheet in crater Np, the sand extending beyond the edges of the main dune field on the intercrater plains (i.e., the sand sheet) is indistinguishable in nighttime IR images.

[47] Beyond the dunes, the nighttime IR mosaic (Figure 5c) shows a great deal of spatial variability that is not readily apparent in either the MOC WA mosaic or the daytime IR mosaic. In contrast to the craters surrounding crater Np (see Figure 3c), most of the craters in Figure 5c have dark (cool) floors. The largest two craters contain bright (warm) patches in their interiors. These craters are roughly the same size as those just east of crater Np (see Figures 3a and 3c), which also have bright (warm) patches in their interiors (note difference in scale between Figures 3 and 5). This correspondence between crater size and nighttime crater floor temperature suggests a progression from larger (>~20 km), bright-floored craters to a mid-range (~10–20 km) of craters with floors that are partially bright to smaller (<~10 km), dark-floored craters.

[48] The nighttime IR mosaic (Figure 5c) shows a great deal of spatial structure between the craters. Night-bright (warm) material appears as filamentary, irregular patches

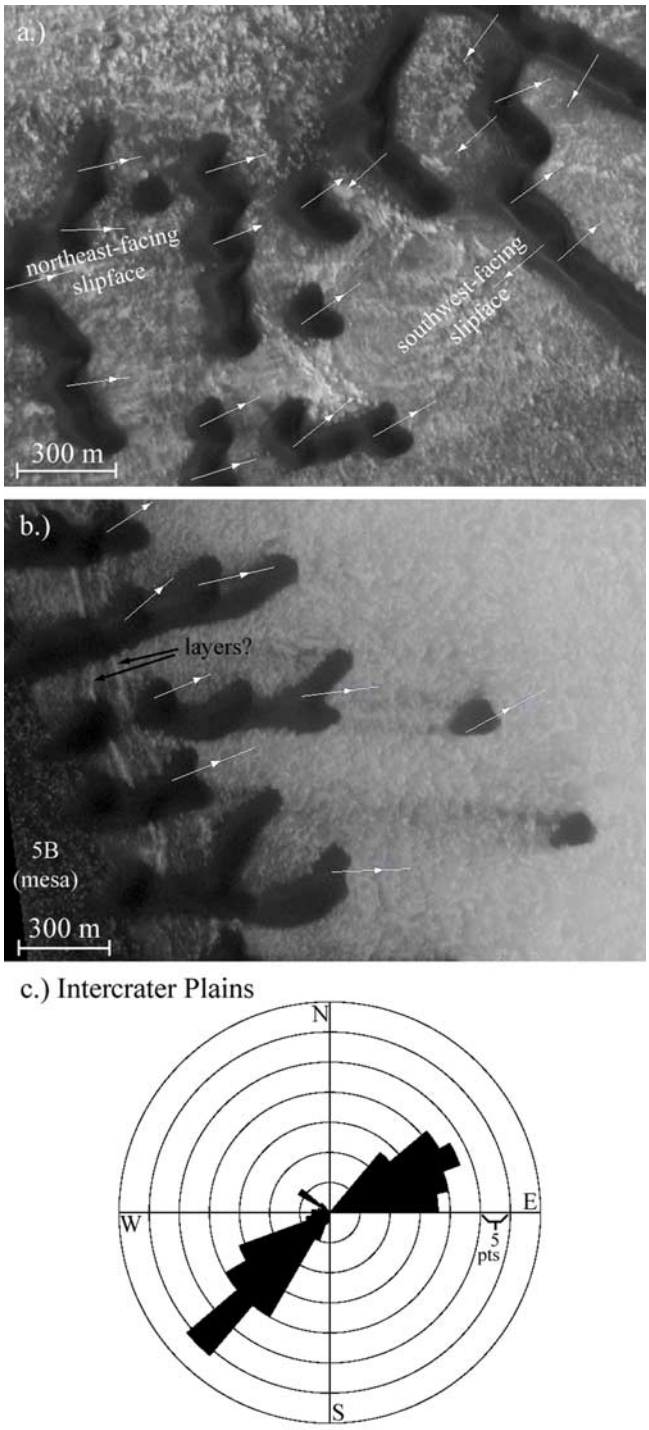

Figure 6. MOC NA images of Intercrater Plains Dunes: (a) Portion of MOC narrow-angle image E12/00457 from the main dune field, showing a general lack of sand cover between the dunes and opposing slipfaces. (b) Portion of MOC narrow-angle image E10/00456 showing dunes on the eastern edge of a mesa (labeled "5B") that is bright in the nighttime IR mosaic. Note rough texture of mesa and lineations under the dunes that may be exposed layers on the mesa wall. (c) Rose diagram of intercrater dune field slipface orientations (indicating downwind direction).

(labeled "5A"), as 5–8 km diameter subround spots (labeled "5B"), and as other smaller patches. Most of these areas appear very subtly, if at all, in both the MOC WA and daytime IR mosaics. Both of the two areas labeled "5A" that are covered by daytime IR images are slightly dark (cool) relative to the surrounding terrain, consistent with the pattern found on the intercrater plains near crater Np (see "3B" in Figures 3b and 3c)). However, the three subround spots vary in contrast in daytime IR images: the northernmost spot appears slightly darker (cooler) than the surrounding terrain and the southern two spots show no temperature contrast with the surrounding terrain. Of all of these nighttime-bright features, none clearly stands out in the MOLA data (Figure 5d), except for the northernmost subround spot (5B), which appears to be a mesa. Unfortunately, no MOC NA coverage of these areas is available to discern why the daytime infrared contrast varies in these areas.

3.2.2. Intercrater Plains: MOC Narrow-Angle Images

[49] The MOC narrow-angle images reveal much about the dunes on the intercrater plains. Figures 6a and 6b show two examples of dunes in this area. Figure 6a shows dunes at the northern end of the main dune field. The dark dunes are spaced widely apart, with the underlying surface clearly showing through and covering at least 50% of the area spanned by the dune field. This underlying surface is not apparent in the mosaics: the area of Figure 6a is within the bright (warm) region in the daytime IR mosaic (interpreted above as covered by sand), and few gaps in dune coverage are visible in the MOC WA mosaic. It is possible that small amounts of dark sand fill small cracks in the interdune areas, contributing to a lower overall albedo and higher overall daytime temperature within the dune field. Alternatively, active sand saltation in the area between the dunes may scour away any higher albedo dust, revealing an underlying surface that has a lower albedo (and thus a higher daytime temperature) than the surrounding dust-covered terrain.

[50] Figure 6b shows dunes on the east side of a subround spot interpreted as a mesa (labeled "5B" in both Figure 6b and Figure 5). The surface of the mesa (5B) in the MOC NA image has a mottled surface similar to that within the sand sheet in Crater Np, shown in Figure 4c. This surface is interpreted as dark sand accumulations with small ($\leq$10 m) higher albedo boulders or knobs poking through the sand cover. On the eastern wall of the mesa, dark dunes have formed on top of a surface brighter than that on the top of the mesa. The dunes cover a lineated surface, suggesting that layered material may be exposed in the mesa walls. East of the mesa, the dunes thin and become smaller, and the underlying surface grows much brighter.

[51] The dark dunes have a similar size and morphology with respect to those in crater Np. In the main dune field (Figure 6a), dunes have a barchanoid or transverse planform. White arrows indicate inferred slipface orientations. As with the crater Np dunes, there are two main dune slope directions that are interpreted as slipfaces, both of which are apparent in Figure 6a. One slipface is oriented toward the northeast, suggesting formative winds blowing from the southwest. The second slipface is oriented toward the southwest, suggesting formative winds from the northeast. The dunes in Figure 6b, west of the main dune field, all show slipfaces oriented toward the northeast. Figure 6c

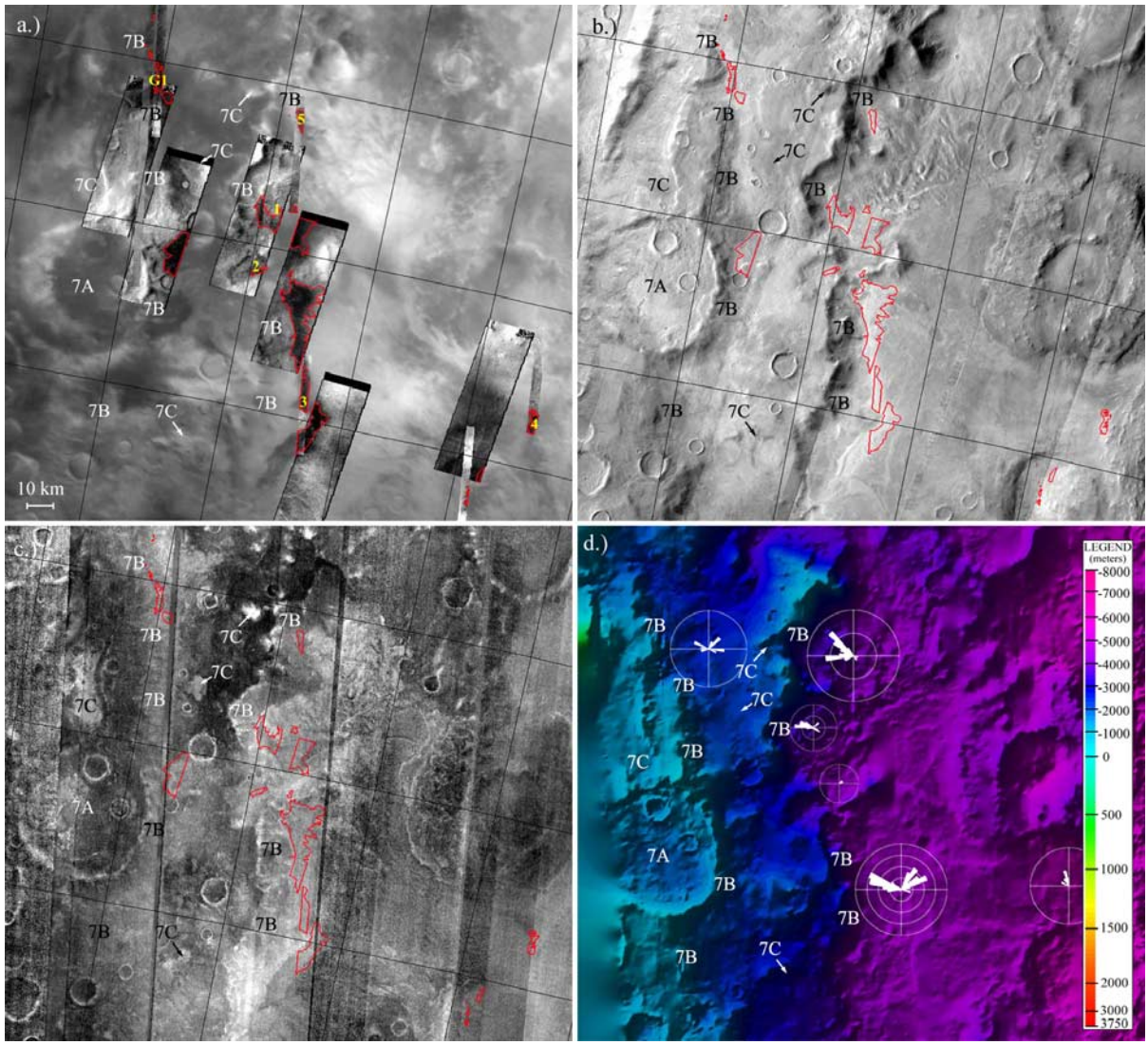

Figure 7. Several dune fields in the Hellespontus Montes abutted against east-facing cliffs stepping down into Hellas Planitia. Like the dunes in Figure 5, these are also not located within craters. (a) MOC WA mosaic with five MOC NA images superimposed (JMARS), (b) THEMIS daytime IR mosaic (JMARS), (c) THEMIS nighttime IR mosaic (JMARS), and (d) MOLA DEM and shaded relief (ArcView), including rose diagrams from individual dune fields. Dunes in MOC narrow-angle images outlined in red. A crater with a possible sand sheet is labeled 7A, cliffs are labeled as 7B, and patches that are bright in the nighttime IR mosaic are labeled 7C.

shows a rose diagram of (downwind) slipface orientations from all of the dunes on the intercrater plains shown in Figure 5 (not including those in the small crater south of the main dune field). Like the dunes in crater Np, the dunes on the intercrater plains appear to reflect two opposing winds. These winds are rotated ~45° counterclockwise from those in crater Np (compare Figures 6c and 4b).

3.3. Hellas Dunes

3.3.1. Hellas Dunes: Mosaics

[52] The western rim of the Hellas Planitia is another area in the Noachis Terra quadrangle containing dark dunes. More than half a dozen dune fields lie just east of the walls of cliffs stepping down into the Hellas basin (see Figure 7). A few smaller dune fields lie further inside Hellas Planitia. Like the dune fields discussed in section 3.2, these dune fields are not located in craters. Because most dune fields in Noachis Terra are located on crater floors, the dunes on the edge of the Hellas basin are unusual. The combination of sand supply, wind velocities, and surface roughness that elsewhere has caused sand to accumulate in craters apparently operates differently on the edge of Hellas Planitia, causing dunes to form at the foot of cliffs rather than in nearby craters.

[53] In Figure 7a, THEMIS VIS and MOC NA images of dunes are superimposed on a MOC WA mosaic. Dune fields visible in VIS and MOC NA images are outlined in red. The dune fields appear as dark areas on a brighter terrain, although there are other relatively dark areas that are not dune fields. For example, the ~50 km diameter crater on the west edge of Figure 7a has a floor that appears mostly dark in the MOC WA mosaic (labeled as "7A"), however the two

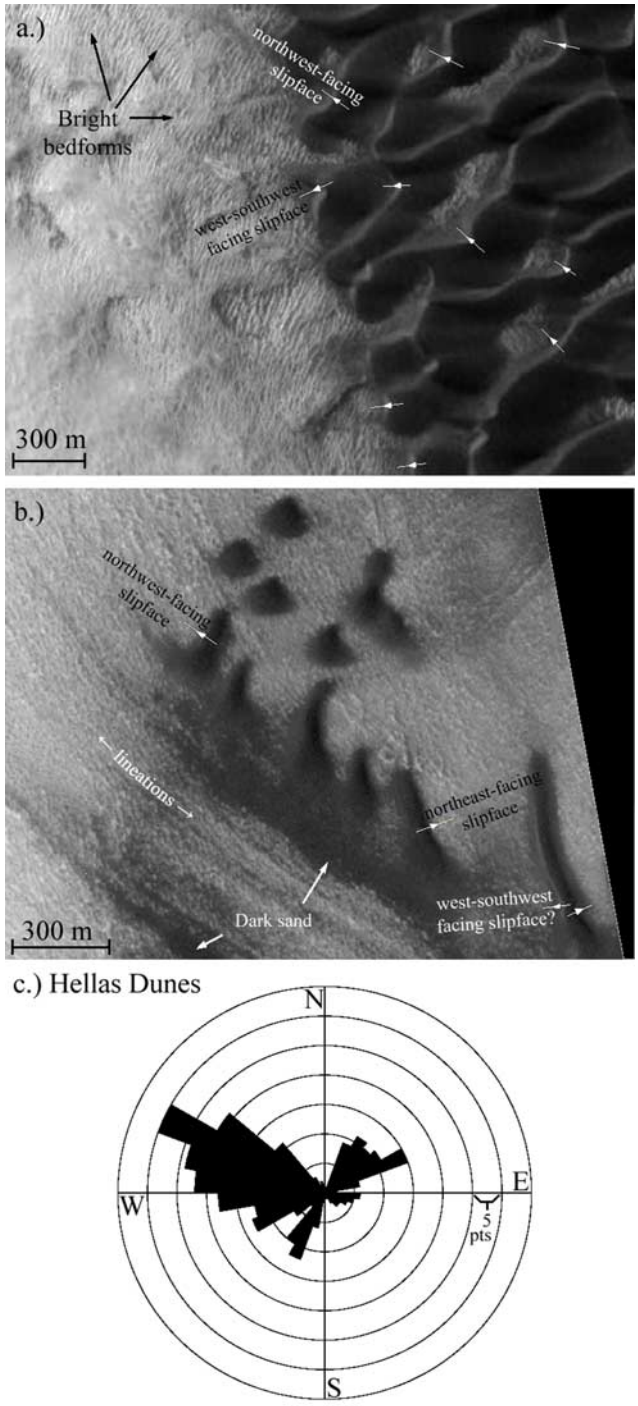

Figure 8. MOC NA images of Hellas Dunes: (a) Portion of MOC narrow-angle image E18/00031 showing the western edge of one of the large dune fields against the Hellespontes cliffs. Note the differing slipface orientations and the many small bright bed forms that seem to be aligned with the most common slipface orientations in Figure 8c. (b) Portion of MOC narrow-angle image R11/01487 showing dunes on the floor of Hellas Planitia. Note that these dunes are more widely spaced than those against the Hellespontes cliffs, but that they still show slipface orientations common to the area. (c) Rose diagram of intercrater dune field slipface orientations (indicating downwind direction).

available MOC NA images of this crater floor are of low quality or low resolution, making it difficult to determine why the crater floor is dark. It is possible that part of this crater floor is covered by a dark sand sheet. In the daytime IR mosaic (Figure 7b), the dune fields appear as slightly brighter (warmer) areas, but generally there is not much contrast between the dune fields and the surrounding terrain. This may be in part due to the presence of dark sand sheets outside the dune fields (e.g., area "7A") that heat up during the day to a temperature comparable to that on the dunes. In the nighttime IR mosaic (Figure 7c), the dunes are difficult to see, appearing as fairly uniform regions of mid-range temperatures. This is consistent with observations of dune fields in crater Np and on the intercrater plains.

[54] Beyond the dune fields, the surrounding terrain in Figures 7a, 7b, and 7c is similar to that described for crater Np and the intercrater plains. Most of the intercrater plains just outside of Hellas appear dominated by temperature differences from slopes and shading in the daytime IR mosaic (Figure 7b). In the nighttime IR mosaic, more spatial structure is present. All of the craters less than ~15 km diameter in Figure 7c have dark (cool) floors in the nighttime IR mosaic, and the large ~50 km diameter crater at the west edge of the figure has patches of bright terrain in its floor. This pattern differs somewhat from that observed near crater Np and the intercrater plains, where craters >~20 km all have bright floors and those <~10 km all have dark floors, and those craters in between have patches of bright and patches of dark terrain in the nighttime IR mosaic.

[55] Out on the intercrater terrain in Figure 7c, the nighttime IR mosaic shows a number of bright (warm) areas. The largest swaths (labeled "7B") correspond to two east-facing cliffs that step down into Hellas. This hilly terrain is known as the Hellespontus Montes. In the daytime IR mosaic, these cliffs appear as shaded slopes (see Figure 7b), but they are difficult to discern at all in the MOC WA mosaic (see Figure 7a).

[56] The remaining nighttime-bright patches on the intercrater plains (labeled "7C") are mostly located on the high plains west of the lowest (eastern) Hellespontus cliff. These patches are similar to those found on the intercrater plains elsewhere in Noachis Terra (see Figures 3c and 5c). Like the other night-bright patches, these are barely visible in the daytime IR mosaic as slightly cooler areas. However, they are almost impossible to spot in the MOC WA mosaic.

3.3.2. Hellas Dunes: MOC Narrow-Angle Images

[57] The MOC narrow-angle images provide detailed information of the dark dunes that is not visible at the scale of the mosaics. Figure 8 shows details of dunes on the edge of and within the Hellas basin. The dunes in Figure 8a are at the western edge of one of the dune fields that sits at the foot of a cliff stepping down into Hellas. Individual dark dunes in Figure 8a are similar in size to those in crater Np and on the intercrater dunes. However, this dune field in Hellas has smaller interdunes than the dune fields discussed above. The dunes also tend to show only one slipface on each dune, although the double-sided morphology does appear elsewhere within the Hellas dune fields. The interdunes and terrain surrounding the dune field are bright relative to the dark dunes and appear free

of dark sand sheets, such as those observed near the dunes in crater Np and the intercrater dune fields (see Figures 3 and 5).

[58] A few dune fields have also formed out on the floor of Hellas Planitia (see Figure 8b). These dunes are generally more widely spaced than those that abut against the Hellespontus walls. The terrain south of the dunes in Figure 8b appears to be rough, and it is likely covered with either boulders or erosional knobs. Dark sand covers the floor in some areas between the highstanding boulders or knobs, accentuating a subtle lineation in the terrain. The lineation is suggestive of exposed layers, similar to suggested layering on a free-standing mesa on the intercrater plains (compare Figure 8b and Figure 6b).

[59] The dunes in Hellas Planitia have slipface orientations similar to those of the more typical dunes of Noachis Terra, but with more variability. Two possible slipfaces are visible in Figure 8a (shown as white arrows), one oriented toward the northwest (suggesting a formative wind from the southeast), and another oriented toward the west-southwest (suggesting a formative wind from the east-northeast). Two or three slipface orientations are visible in Figure 8b, although the planform of the dunes suggests one wind from the west-southwest dominates their morphology. One set of slipfaces is oriented toward the northeast (suggesting formative winds from the southwest) and another is oriented toward the northwest (suggesting formative winds from the southeast). The dune in the southeast corner of Figure 8b has what is interpreted in this work as two slipfaces on either side of a reversing transverse dune. This double-sided morphology is similar to that seen in crater Np (see Figure 4a) and in Proctor Crater [*Fenton et al.*, 2005]. The western side of this dune has a slipface that may be oriented toward the west-southwest, suggesting that three winds influence the dunes in this area.

[60] Bed forms that are smaller (~20 m spacing) and brighter than the dark dunes are visible just off the edge of the dune field. Similar bright bed forms have been observed near the dark dunes in Proctor Crater [*Fenton et al.*, 2003, 2005], and they are common on much of the Martian surface [*Malin and Edgett*, 2001]. *Wilson et al.* [2003] suggested that these features are similar to terrestrial granule ripples. Such ripples run transverse to the local sand-moving winds, so it is possible that these bed forms are aligned with the northwest-facing slipfaces in the dark dunes.

[61] Figure 8c shows a rose diagram of each of the dune slipface orientation measurements made for each of the dunes in the Hellas region (areas outlined in red in MOC NA images in Figure 7). Overall, the slipfaces of the dunes in Hellas show much more variation than those of crater Np or the intercrater plains (compare with Figures 4b and 6c). The rose diagram suggests that as many as (and perhaps more than) four wind directions affect dune morphology on the west edge of Hellas Planitia. The most commonly found slipface is oriented toward the west-northwest, but it varies in orientation from the northwest to the west-southwest. This dominating slipface could indicate winds that vary from dune field to dune field on the edge of Hellas, possibly deflected by local topography. Alternatively, it may represent two (or more) more unidirectional winds that overlap at the 10° binning resolution of the rose diagrams. In Figure 7d, wind roses from each of the six dune fields (that collectively compose the wind rose in Figure 8c) have been shown over their respective locations in Hellas Planitia. The west-southwest to northwest slipfaces are common to almost all of the dune fields, varying in direction slightly from one dune field to the next. In one dune field, these slipfaces are divided into two directions: one directly northwest and one almost due west. In other dune fields, slipfaces reflect only one such wind that varies in direction slightly from one dune field to another. It is likely that both possible situations listed above are occurring: that more than one wind from the east to southeast influences the Hellas Planitia dunes, and that each wind is influenced by local topography.

3.4. Rabe Crater: Dunes and Layers

3.4.1. Rabe Crater: Mosaics

[62] Rabe Crater is a ~100 km diameter crater, located at 35°E, 44°S, roughly 300 km east northeast of crater Np (see Figure 9). Rabe Crater contains a ~50 km × ~35 km dune field, one of the largest in Noachis Terra. Most of the dune sand has accumulated in a large, roughly circular, ~50 km diameter pit. This is in contrast to crater Np, in which a small dune field is located some distance from much smaller, shallower crater floor pits. In Rabe Crater, the arrangement of dunes within a large pit on the crater floor is one of the few such examples in Noachis Terra. It is this contrast with crater Np, as well as distinctive layering in pit walls (discussed below) that makes Rabe Crater a region of interest.

[63] The dune field (outlined in red in Figure 9) appears as a dark mass in the MOC WA mosaic, with individual dunes nearly resolved. Many MOC NA images cover the dunes in Rabe Crater, but the dune field as a whole is best shown at the resolution of MOC WA images. As is typical for dunes in Noachis Terra, the dunes in Rabe Crater appear bright (warm) in the daytime IR mosaic (Figure 9b), and intermediate in the nighttime IR mosaic (Figure 9c).

[64] Most of the floor of Rabe Crater appears bright (warm) in the nighttime IR mosaic (Figure 9c). However, the large pit (labeled "9A"), in which most of the dune field is located, is darker (cooler) than the crater floor and the dune field. The daytime IR appears to be largely dominated by topographic effects, providing no additional information on the nature of the crater floor and pit material. However, the nighttime IR data suggests that there is a difference in material properties of the relatively nighttime-bright crater floor and relatively nighttime-dark pit.

[65] Outside Rabe Crater on the intercrater plains, most of the surfaces appear dark in the nighttime IR mosaic. A few irregular spots appear nighttime-bright (labeled "9B"). Although these areas are not apparent in the MOC WA mosaic, several of these places are darker (cooler) in the daytime IR mosaic, suggesting that these nighttime-bright spots are regions of higher thermal inertia than most of the intercrater plains. Note also that all of the smaller craters (≤~15 km) on the intercrater plains have dark (cool) floors, in contrast with the much larger Rabe Crater. This pattern is similar to that seen on the intercrater plains in Figures 3c and 5c.

3.4.2. Rabe Crater Layers: MOC Narrow-Angle Images

[66] Rabe Crater has been well covered by MOC. Its images reveal a large, tall dune field with few interdunes.

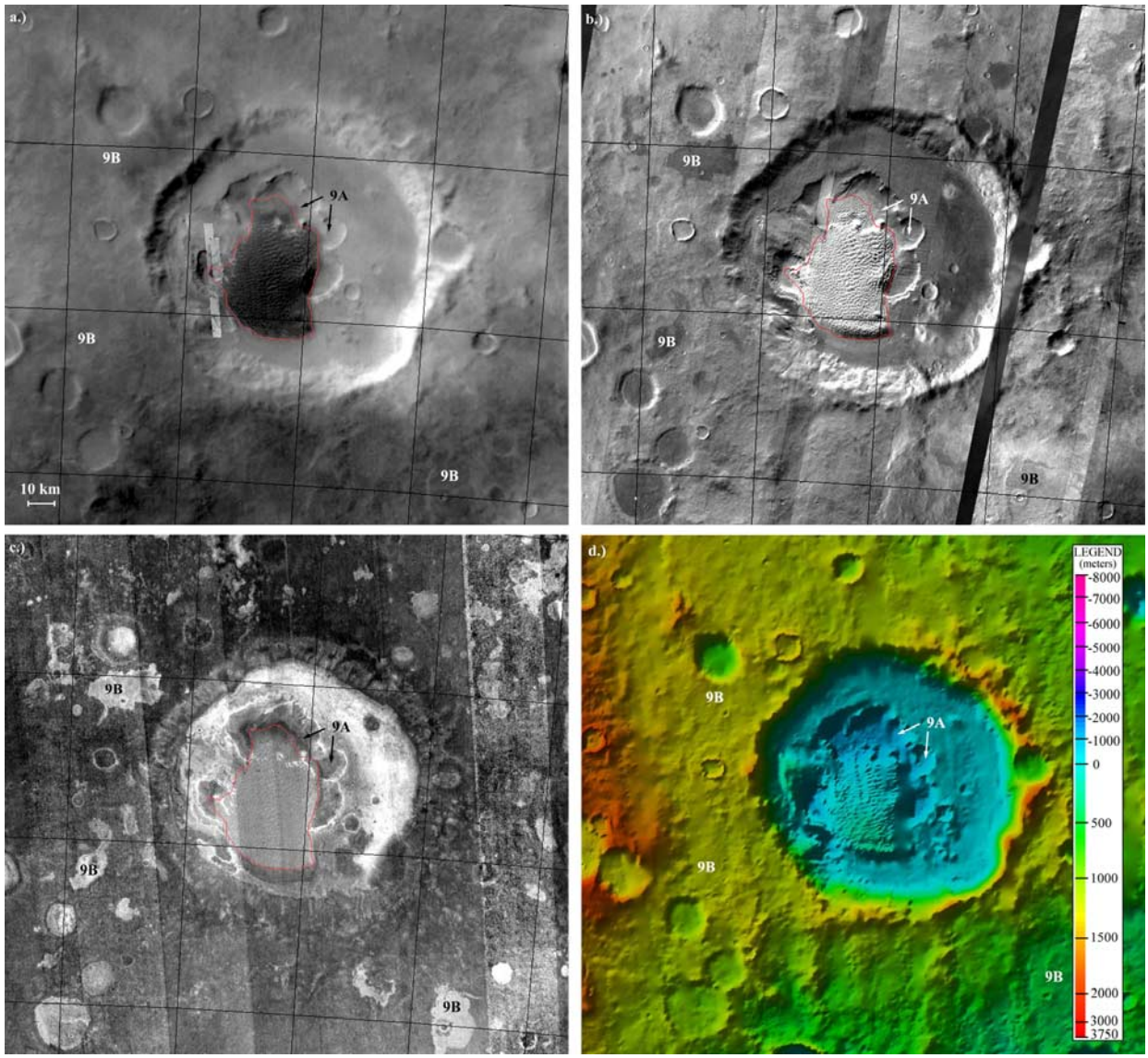

Figure 9. Large dune field and pit on the floor of Rabe Crater. (a) MOC WA mosaic with five MOC NA images superimposed (JMARS), (b) THEMIS daytime IR mosaic (JMARS), (c) THEMIS nighttime IR mosaic (JMARS), and (d) MOLA DEM and shaded relief (ArcView). Dunes in MOC narrow-angle images outlined in red. Note how the pit (9A) is dark (cool) in the nighttime IR mosaic, but the flat crater floor is bright (warm). Note also the many spots on the intercrater plains that are bright (warm) in the nighttime IR mosaic (9B), but that are difficult to spot in the MOC WA mosaic and are dark (cool) in the daytime IR mosaic.

However, the images of the crater floor and pit walls are just as interesting, revealing a complex history of sedimentation and erosion that lies stratigraphically beneath the dune field. Because erosional patterns near the dune fields may give clues to the sand transport pathways that built the dune fields, it is this terrain underlying the Rabe Crater dunes that is discussed here.

[67] Figure 10a shows a MOC WA mosaic of the western side of Rabe Crater with one superimposed THEMIS VIS image. Close inspection of the pit walls show that several layers are present. Figure 10b shows the same area as Figure 10a with MOC NA images superimposed. The MOC NA images were used to identify different layers of material present in the Rabe Crater pit. These layers are outlined in white and labeled with unit numbers 1 through 4. Each unit has its own distinctive morphology and thickness. It is possible that unconformities exist between some or all of these layers.

[68] The lowest layers, units 1 and 2, are shown in Figure 10c. Two MOC NA images show the western edge of the dune field (labeled "dark dunes"), as well as the lower portion of the western wall of the pit. In the pit wall, two different units are exposed: the lower (unit 1) is unlayered and gullied and the upper (unit 2) is layered without gullies. The presence of layered materials strongly suggests that these are sediments that accumulated in Rabe Crater after the crater's formation, rather than original crater floor material. The upper, layered unit

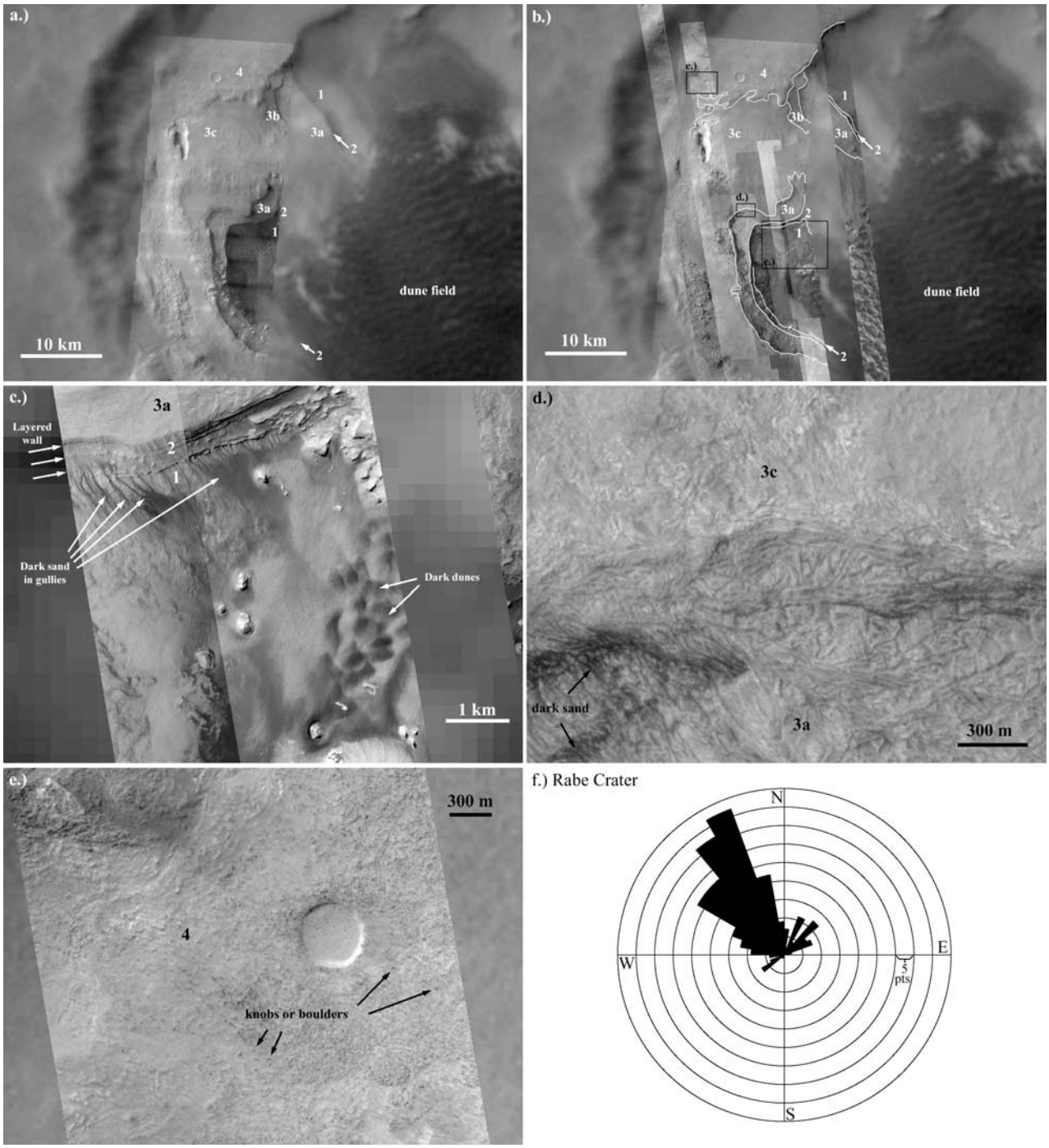

Figure 10. (a) Layers on the pit wall in Rabe Crater, labeled 1 through 4 (oldest to youngest). (b) Same area as Figure 10a, but with MOC narrow-angle images superimposed. White lines show contacts between units 1 through 4. Black boxes show the locations of Figures 10c, 10d, and 10e. (c) Bottom of Rabe Crater pit, showing lower, gullied layer (unit 1) carrying dark material (probably sand) down to the pit floor and resistant layers above (unit 2) that may be shedding the dark material. (d) Layers with an etched appearance and small accumulations of dark material (units 3a–3c). (e) Rough surface with either boulders or knobs (unit 4), capping the strata and forming much of the flat floor of Rabe Crater. (f) Rose diagram of Rabe Crater dune slipface orientations (indicating downwind direction).

appears to be more resistant than the lower, gullied unit. Dark material is present in most of the gullies in the pit wall, and some of the dark material is connected to dark dunes on the pit floor below. This dark material is interpreted as the same dark sand that comprises the Rabe Crater dunes.

[69] The smaller black boxes in Figure 10b show the locations of Figures 10d and 10e), which illustrate the

surface textures of units 3 and 4. Unit 3 has an etched appearance (see Figure 10d). Three adjacent layers, all containing a similar etched texture, and without a distinct contact from one layer to the next (e.g., see contact between units 3a and 3c in Figure 10d), have been grouped into unit 3 and divided into subunits 3a, 3b, and 3c. Unit 3b is not apparent in all MOC NA images, suggesting that either this layer is not present across all of the studied terrain, or that the contacts between units 3a, 3b, and 3c are not always possible to discern in the images. There are small accumulations of dark material in some areas of unit 3 that are interpreted here as dark sand. Unit 4 comprises most of the flat floor of Rabe Crater outside the pit. This unit has a rough surface that is interpreted here as either knobby or bouldered (see Figure 10e).

[70] In the nighttime IR mosaic (Figure 9c), there are contrasts in temperature from one unit to the next that are not apparent in either the daytime IR mosaic or the MOC WA mosaic. Units 2 through 4 correspond to fairly bright (warm) surfaces, and unit 1 is the dark pit wall discussed above (labeled "9A" in Figure 9c). In particular, there is a night-bright ring around the rim of the pit, corresponding to the thin layers of unit 2. This bright ring is not apparent everywhere, such as along the south edge of the pit where dunes obscure the thermal signature of the pit walls.

3.4.3. Rabe Crater Dunes: MOC Narrow-Angle Images

[71] The morphology of the Rabe Crater dune field is not discussed in detail in this work, but it is worth comparing their slipface orientations with those of other dunes in Noachis Terra. Figure 10f shows the rose diagram showing the (downwind) orientations of transverse and barchan dunes in Rabe Crater. These dunes are dominated by northwest-facing slipfaces; however, minor slipfaces oriented to the northeast and southwest are present. Northwest-facing slipfaces dominate the Hellas dunes (see Figure 8c), although in Rabe Crater they are rotated $\sim$30° to the north relative to the Hellas dunes. Northwest-facing slipfaces are not present in crater Np (see Figure 4b), but they are present in a few dunes on the intercrater plains (see Figure 6c).

3.4.4. Rabe Crater: Volumes

[72] Relative to crater Np, both the Rabe Crater pit and dune field are much larger. However, the same question may be asked: is the dune sand volume greater than that of the pit in Rabe Crater? If this is the case, then it is clear that not all of the dune sand could be derived from the pit alone. If the dune sand volume is less than that of the Rabe Crater pit, then the pit materials cannot be ruled out as the sole source for dune sand.

[73] The Rabe Crater dunes rest upon high relief topography, and without knowledge of the underlying surface structure, it is impossible to correctly calculate the volume of dune sand. The Rabe Crater situation is different from that in crater Np, in which the dune field rests upon a fairly flat plain. Some of the Rabe Crater dunes are located in the pit, and some of the dunes spill out onto the flat crater floor surrounding the pit (see Figure 9d). The complexity of the terrain may be dealt with by measuring the volume of sand above the height of the pit walls and comparing it to the cavity volume below the height of the pit walls. It is clear that the dunes currently located in the pit are capable of filling a portion of its volume. The question is whether the remaining dunes above and beyond the pit could fill the remaining cavity.

[74] Using the IDL routine GRIDVIEW, the volume of dune sand above the pit wall height of -300 m was calculated at $\sim$204 km^3, and the cavity volume of the pit below a height of -300 m was found to be $\sim$680 km^3. As with the crater Np, it is possible that the dunes are poorly sampled by MOLA, and the dune volume is underestimated. However, the dunes in Rabe Crater are much larger than those in crater Np, thus they are less likely be undersampled. Even if the dune volume is underestimated by a factor of two, the dune sand cannot fill all of the cavity space in the Rabe Crater pit. As with crater Np, the pit cannot be ruled out as the sole source for dune sand.

3.5. Crater Xn: Dunes and Layers

3.5.1. Crater Xn: Mosaics

[75] Crater Xn is a $\sim$60 km diameter crater located at the western edge of Noachis Terra, at 5°E, 45.5°S (see Figure 11a). The white box shows where Figure 12 is located. Crater Xn is quite distinct from most typical craters: its topography appears to be inverted. Rather than having a raised rim and low interior, crater Xn has a floor that is not far below ($\sim$700 m below) the surrounding intercrater plains and rim that has almost disappeared. Instead of a rim, most of the perimeter of the crater is defined by a series of arcuate depressions that are as much as $\sim$2200 m below the interior crater floor and as much as $\sim$2700 m below the surrounding intercrater plains. Crater Xn may have been almost completely filled at some point in the past. Later, a large amount of material was removed from a region ringing the interior of the rim. Of the remaining filled crater floor, a few smaller pits and a number of fractures are present. *Malin and Edgett* [2000] used this crater as an example of sedimentary erosion in its early stages (see their Figure 11B). It is not clear how far in the past the infilling or subsequent erosion of material in crater Xn occurred, but it predates the formation of the dunes present in the crater's depressions. Although crater Xn does not contain many dunes, its state of infill and subsequent erosion make it a unique place to search for sand transport pathways. The small red areas in Figure 11a indicate the dunes located in crater Xn. They are located in either a deep central pit (e.g., the red area inside the white box) or in a shallow, highly eroded crater on top of the crater Xn floor.

[76] The daytime IR mosaic shows variations in temperature created by topography, and no obvious bright (warm) dune fields or dark (cool) intercrater plains spots, such as those visible in other areas discussed above. However, the nighttime IR mosaic shows more detail relating to the properties of the surface. Most of the crater floor and the surrounding intercrater plains are uniformly and relatively dark (cool). The walls of the arcuate and central pits are quite bright (warm). The floors of the pits are intermediate in temperature, and show spatial structure that probably corresponds with topographic features on the pit floors.

3.5.2. Crater Xn: MOC Narrow-Angle Images

[77] Figure 12 shows an area within an eroded pit in the center of the crater floor. This is a situation very similar to

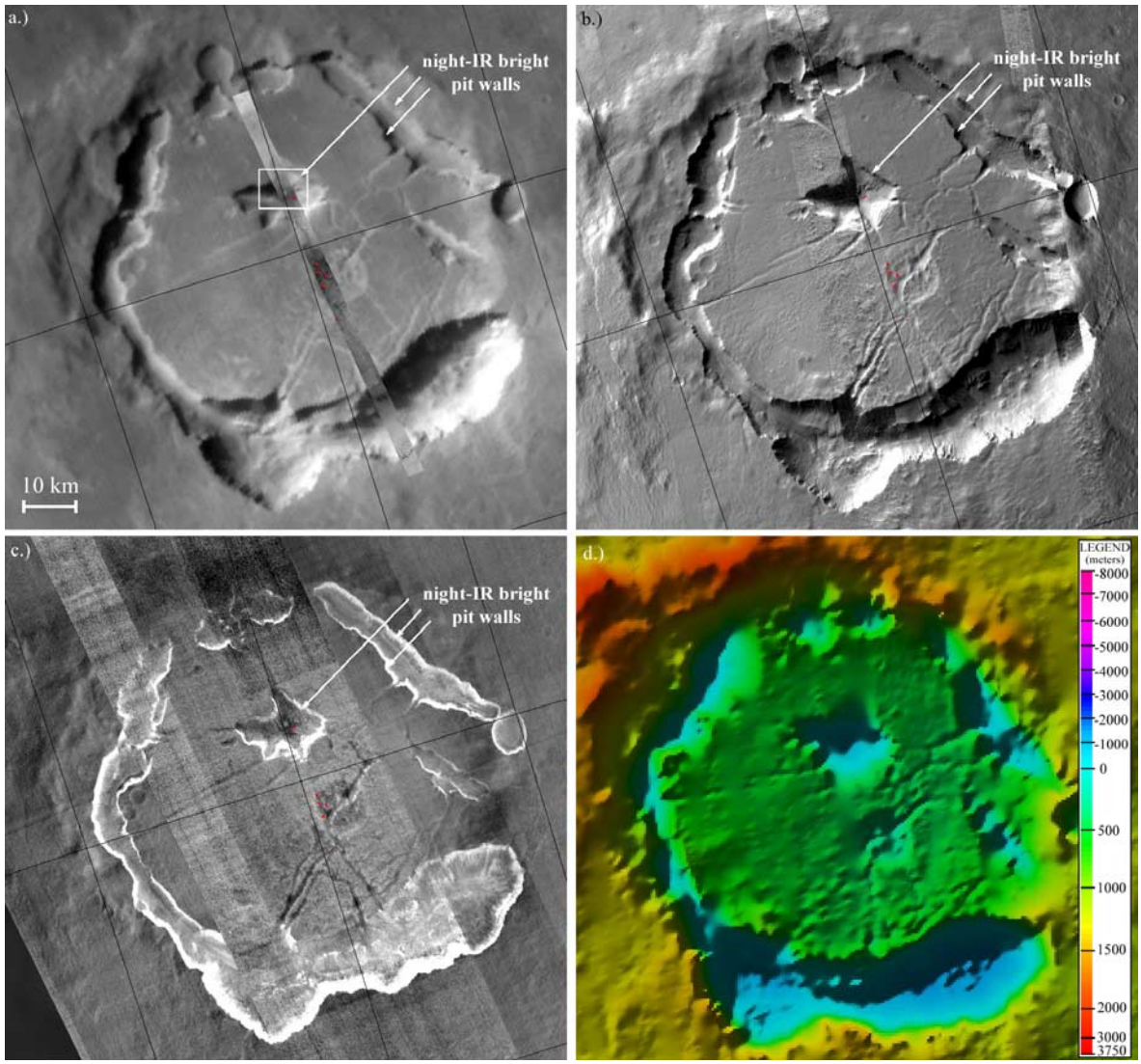

Figure 11. Crater Xn, almost completely filled with sediments, is identifiable as a crater only because arcuate pits ringing the crater walls have been eroded. (a) MOC WA mosaic with five MOC NA images superimposed (JMARS), (b) THEMIS daytime IR mosaic (JMARS), (c) THEMIS nighttime IR mosaic (JMARS), and (d) MOLA DEM and shaded relief (ArcView). Dunes in MOC narrow-angle images outlined in red. Note how the upper walls of the pits are bright in the nighttime IR mosaic.

that shown in Rabe Crater in Figure 10c. The walls of the pit show two different layers: an upper, resistant, layered unit and a lower, gullied unit containing dark material. This dark material is interpreted to be dark sand. In the floor of the pit are a few dark dunes. The upper unit is similar to unit 2 and the lower unit is similar to unit 1 of the Rabe Crater pit walls.

[78] The nighttime IR images of crater Xn also show a situation very similar to that of Rabe crater. In Figure 11c, the pit walls ringing the interior of the crater, as well as the central pit where the dark dunes are located, both show the two layers very clearly. The upper, resistant, layered unit appears bright (warm), and the lower, gullied unit is relatively dark (cool). However, unlike Rabe Crater, the pit walls in crater Xn are not overlain by night-bright etched or blocky layers similar to units 3 and 4. Rather, there is a fairly thin (<~20 m thick) nighttime dark (cool) material.

4. Discussion

4.1. Wind Regime From Dune Slipfaces

[79] *Fenton et al.* [2003] found that the dunes of Proctor Crater (labeled "PC" in Figure 1) displayed three slipface orientations, labeled "primary," "secondary," or "tertiary" according to the size of the area in which they were found within the dune field. The primary slipfaces are oriented toward the east-northeast, the secondary slipfaces are oriented toward the west-northwest, and the tertiary slipfaces are oriented toward the west-southwest [see *Fenton et al.*, 2003, Figure 5]. This multidirectional wind regime corresponds well with the observed combination of reversing

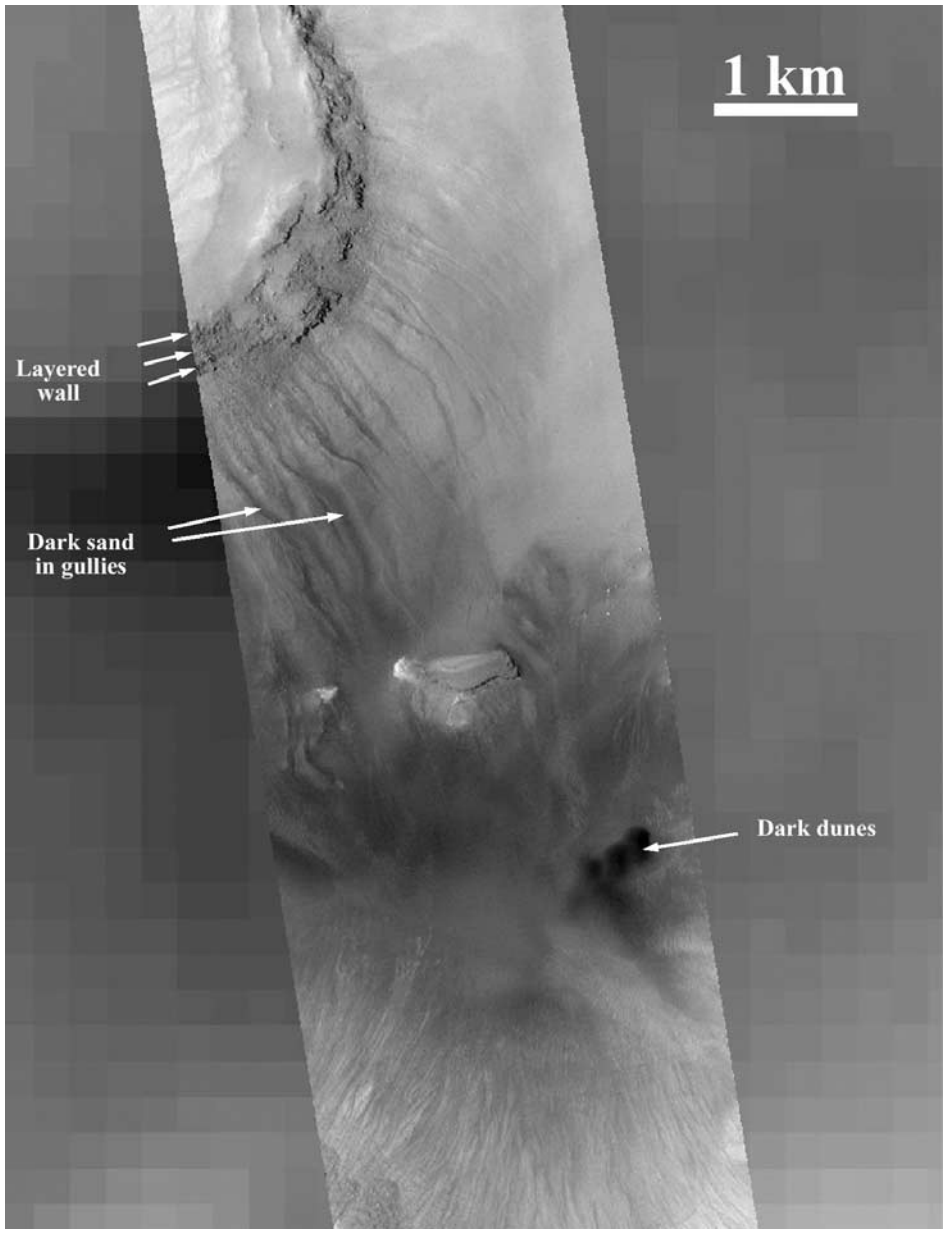

Figure 12. Layers on the pit wall in crater Xn, showing two units that are very similar to Rabe units 1 and 2 (compare with Figure 10c). The upper, resistant layered unit appears to be shedding dark sand down gullies in the lower, less resistant unit to the dunes on the pit floor. Could this be a source of sand for the Noachis Terra dunes?

transverse, double-sided barchan, and star dunes that are present in the Proctor Crater dune field. If these dunes were formed by regional winds (i.e., winds that extend across a large portion of Noachis Terra or more), then it is reasonable to expect a similar distribution of dune slipface orientations in the measurements made in this study. Conversely, if the Proctor Crater dunes were formed by winds derived from local topography (e.g., slope winds unique to the crater walls), then slipface orientations would probably vary from one dune field to the next, particularly for those dune fields not located in craters (such as those on the intercrater plains and off the edge of Hellas Planitia).

[80] Crater Np is located ~150 km north-northwest of the center of Proctor Crater, and it contains the dune field closest to that of Proctor Crater. Its slipfaces (see Figure 4b) correspond well to two of those found in the Proctor Crater dunes. The most plentiful slipfaces, facing west-southwest, are similar in direction to the tertiary slipfaces from Proctor Crater. A few remaining slipfaces, facing east-northeast, are similar to the primary slipfaces. This correlation strongly suggests that at least two winds that influence the dunes in Proctor Crater are also found in crater Np.

[81] The dune field of Rabe Crater is located ~300 km northeast of the center of Proctor Crater, the next closest dune field to Proctor Crater discussed in this work. The dominant slipface orientation in the Rabe Crater dunes is to the northwest (see Figure 10f). It is possible that these slipfaces are created by the same winds that produce the

secondary slipfaces in Proctor Crater, although they are rotated ~45° clockwise relative to the Proctor Crater slipfaces. If these slipfaces are produced by the same regional wind, they may have been deflected by local topography, such as the large pit that is unique to the Rabe Crater floor. Because these slipfaces are so prevalent throughout the dune field, it is possible that a southeast wind was responsible for transporting sand into the dune field. However, no sand streamers, dunes, or drifts indicative of a transport pathway are visible on the southern rim or directly south of Rabe Crater (although high resolution images here are sparse). If such a transport pathway ever existed, it is now buried or eroded. The minor slipfaces oriented to the northeast and southwest in Rabe Crater (see Figure 10f) may correspond, respectively, to the primary and tertiary slipfaces observed in Proctor Crater. As with crater Np, the dune slipfaces of Rabe appear similar to those of Proctor Crater.

[82] The next closest dune field to the Proctor Crater dunes is that on the intercrater plains, located ~350 km northeast of Proctor Crater and ~40 km west of the edge of Hellas Planitia. The most common slipfaces, oriented to the southwest (see Figure 6c), may correspond to the tertiary slipfaces observed in Proctor Crater, although they are rotated relatively ~30° counterclockwise. The other dominating slipface orientation in the intercrater plains dunes compares very well with the primary slipfaces observed in Proctor Crater. As with the intracrater dunes discussed above, the intercrater plains dunes show similarities to those measured in Proctor Crater. This is perhaps the best evidence that the dune-forming winds are regional rather than local; their influence of dune morphology both on the floors of craters and out on the intercrater plains strongly suggests that these winds cannot be driven from local topography alone.

[83] The dunes on the western edge of Hellas Planitia are located ~650 km northeast of Proctor Crater. The dominant slipface orientation ranges from west-southwest to northwest (see Figure 8c). As discussed in section 3.3.2, this spread in slipface orientation likely reflects two factors: deflection from local topography and two or more dune-forming winds that overlap on the rose diagram. This dominant orientation compares well with both the secondary and tertiary slipfaces observed in Proctor Crater. The second most dominant slipfaces in the Hellas dunes are oriented to the northeast, possibly corresponding to the primary slipfaces from the Proctor Crater dunes. The third most common slipfaces are oriented to the south-southwest; these could be produced by the same winds that create the tertiary slipfaces in Proctor Crater, although they are rotated relatively ~45° counterclockwise and it is difficult to explain how two distinct winds observed in Hellas dunes could turn into the single tertiary slipface orientation observed in Proctor Crater dunes. Finally, a minor component of slipfaces oriented to the east-southeast are present in the Hellas dunes, but not found in any other dunes measured in this study. It is likely that the extreme topography of the Hellespontus Montes area and slope winds known to dominate circulation in the Hellas basin [*Joshi et al.*, 1997] affect local wind speed and direction, possibly contributing to the high variability of slipface orientations observed in the Hellas dunes. It is unclear whether the winds that produce Hellas dune slipfaces truly correspond to those that produce the Proctor Crater dune slipfaces, but their similarity is suggestive.

[84] Each of the four sets of dune fields discussed above displays slipfaces that appear to correspond to those found in the Proctor Crater dune field. This strongly supports the idea that the dunes in Noachis Terra are formed by regional winds rather than local winds driven by small-scale topography. However, the proportion of these slipface orientations differs from one dune field to the next. For example, the dominant (what would be considered the "primary") slipface orientation in Rabe Crater corresponds best to the "secondary" slipfaces of Proctor Crater. Furthermore, in some cases the winds appear to rotate by as much as 45° relative to those in Proctor Crater. Thus these regional winds vary spatially in relative strength and direction, probably as a result of a number of factors: both local and regional topography, variations in albedo and thermal inertia, position relative to upwelling and downwelling Hadley currents, influences of local and regional dust storms, and possibly others.

4.2. Short Transport Pathways

[85] In Noachis Terra, the aeolian sedimentary history is different from that typically observed on the Earth. In terrestrial deserts, sand transport pathways can often be traced "upstream" from a dune field to a sand streamer or sand sheet that feeds the dune field. Sometimes the sand transport pathway can be traced upwind beyond this point to further dune fields and sand sheets and possibly finally to a sand source. This is not the case with MOC WA, daytime IR, or nighttime IR mosaics, which reveal the Noachis Terra dunes to be isolated accumulations of sand, with no connections from one dune field to another.

[86] Although some sand sheets and streamers are visible in the MOC WA and daytime IR mosaics, they are relatively short (on the scale of the dune field width) and provide no clear link to upwind sources of sand. No sand sheets are apparent in any of the nighttime IR mosaics, where the dunes themselves are often difficult to identify. This lack of visibility in nighttime IR mosaics suggests that the sand sheets identified in MOC WA and daytime IR mosaics are thermally thin (less than a few centimeters thick). MOC narrow-angle images provide the best information on sand transport pathways.

[87] These images often confirm the presence of dark sand sheets where they are inferred in the mosaics. The presence of boulders or knobs appearing through sand cover in many MOC NA images of dark sandy areas is consistent with relatively thin sand sheets proposed from observations of daytime and nighttime IR mosaics. However, dark sand is more difficult to identify in winter MOC NA images, in which a lower sun angle (i.e., the sun is lower in the sky) and possible frost cover both reduce the contrast of dark sand with the surrounding terrain (see discussion in section 2.2, Figure 2). Furthermore, the coverage of MOC NA images is far from complete in most areas on Mars, including Noachis Terra. These limitations inhibit efforts to map out transport pathways of dark sand.

[88] The general absence of observable sand transport pathways in Noachis Terra has implications for the nature of the pathways themselves. *Fenton et al.* [2005] proposed that

the lack of a sand transport pathway for the Proctor Crater dunes indicates that any previously existing pathways have been either eroded away or buried. No such pathways are evident from data sets that span Noachis Terra, such as thermal inertia maps [*Putzig et al.*, 2005] or MOC WA mosaics (see Figure 1). No sand streamers or small sand drifts are visible in the vast majority of the MOC NA images that (sparsely) sample the intercrater plains of Noachis Terra. However, it is possible such pathways were once widespread, actively carrying sand across hundreds of kilometers, with sinks in the present-day dune fields. The present-day wind may be strong enough to prevent the dune fields from becoming eroded or buried, but too weak to maintain the transport pathways. Alternatively, the sand supply feeding these potential transport pathways may have been limited, and any such transport pathways have disappeared because they "ran dry." If this were the case, then these pathways must now be inactive, allowing more recent surface processes to erode or bury them, obscuring them from view. Although this option cannot be ruled out, another possibility exists: the transport pathways may simply be very short, and the dune sand may be derived from nearby local and/or regional sources, either of which could explain the observed situation in Noachis Terra. If the sources of sand are local, then the transport pathways leading from the sand sources to the dune fields may be very short. If the sand sources are regional, then the dunes will accumulate in areas where the winds converge. In this second case, transport pathways may be difficult to detect if they are ubiquitous (i.e., they may cover so much of the surrounding terrain that they appear indistinct).

[89] Not all dune fields in Noachis Terra are contained within craters. One dune field is located on the intercrater plains, and several dune fields are clustered on the western rim of Hellas Planitia, in the Hellespontus Montes. The possibility of short sand transport pathways suggests that sand sources for these dune fields are located on the intercrater plains. Sand sources for intracrater dune fields may come from within the crater, or perhaps on the nearby intercrater plains (or possibly both).

[90] The presence of dunes on the intercrater plains also suggests that dune fields do not accumulate in craters solely because sand is trapped inside them, prevented from escaping by steep crater walls, as suggested by *Christensen* [1983]. If this were the case, dune fields would be unable to accumulate outside of craters. Other factors, such as sand supply and wind regime, must also dictate why dune fields are common to crater floors. Sand sources preferentially located within craters could explain why few dunes are found on the intercrater plains. Additionally, similar morphology and dune slipface orientations among all of the dune fields studied in this work, regardless of where they are located, suggests that the same dune-forming winds blow across most of Noachis Terra. It is likely that dune fields accumulate where these regional winds, possibly funneled or impeded by local topography, balance one another.

4.3. Possible Regional Deposition

[91] Although sand transport pathways are difficult to detect in the low resolution mosaics, there are a few places in MOC NA images that suggest a possible nearby source for dune sand. Both instances occur within craters: Rabe Crater and crater Xn. These two craters are separated by a distance of more than 1200 km, roughly half the mean width of the Noachis Terra quadrangle, but the similarity of the two cases is striking.

[92] In both crater Xn and Rabe Crater, dark dunes are located near the walls of large pits that have similar physical characteristics. In both cases, dark material interpreted as sand is visible in gullies in a lower, night-dark (cool) layer (unit 1 in Rabe Crater), and that dark material is connected to dark dunes on the pit floors. It is possible that a stratigraphically higher night-bright layered unit (unit 2 in Rabe Crater) is eroding, shedding dark sand that is carried downward by way of the gullies and becomes incorporated into the dune fields. Although the dunes are dark in visible images, the layered units have roughly the same albedo as the surrounding crater floors (see Figures 10a and 11a). Therefore if the dark sand in these two craters is indeed derived from the resistant, night-bright layers exposed in the pit walls, the sand cannot be the sole component of the material in the layers.

[93] Likewise, unit 3 contains accumulations of dark material interpreted as sand (see Figure 10d). In Rabe Crater this unit lies stratigraphically and topographically above unit 2, the layered unit thought to be shedding dark sand directly into the dune field below. The accumulations of dark sand on unit 3 may also be derived from the underlying unit 2, perhaps blown up-strata by the wind. Alternatively, unit 3 may also contain some amount of dark sand that is accumulating in place as this unit erodes.

[94] The similarity between the two sets of wall units in both MOC NA images and nighttime THEMIS IR images is clear: a local sand source is eroding and contributing to the nearby dune field. The fact that the pattern is consistent for two craters that are separated by a large distance from one another ($\sim$1200 km), and that the craters are quite different from one another morphologically, is noteworthy. The larger craters ($>\sim$20 km diameter) in Noachis Terra also have bright floors in the nighttime IR mosaics, and these floors may be composed of a material similar to the night-bright layers in Rabe Crater and crater Xn.

[95] For example, crater Np has a fairly bright floor (in visible light) with a rough surface in MOC NA images (see mottled terrain in Figure 4c and interdunes in Figure 4a). This rough surface may be a material similar to Rabe unit 4. The terrain in the large pit in crater Np has an etched appearance (see Figures 2 and 4d), similar to that of Rabe unit 3. There are accumulations of material interpreted as dark sand in the crater Np pit (see Figure 4d), just as there are accumulations of material interpreted as dark sand in parts of Rabe unit 3 (see Figure 10d). It is possible that the sequence of units in Rabe Crater is repeated in crater Np, and that beneath the floor and pits in crater Np (possibly units 4 and 3, respectively), there is unexposed material similar to Rabe units 1 and 2.

[96] This raises the question of how extensive the Rabe units are across Noachis Terra: could the pit in Rabe Crater be exposing a sequence of sediments that were deposited across all or part of Noachis Terra, or does each crater contain its own distinct set of sedimentary layers?

[97] The sequence of Rabe units is not always consistent with what is observed in other craters. For example,

although pits in crater Xn show units very similar to the Rabe units 1 and 2 (gullied and layered units, respectively), the surface of the flat crater floor above these units is dark in nighttime IR mosaics (see Figure 11c), unlike the nighttime-bright Rabe units 3 and 4. However, this disparity may have an explanation that is consistent with a hypothesis of regional sedimentation: it is possible that units similar to Rabe units 3 and 4 never formed in crater Xn (i.e., these units are not as spatially extensive as units 1 and 2), or that they did form and are now completely eroded away.

[98] Another inconsistency between Rabe Crater and crater Xn must be explained: the difference in the sizes of the dune fields. It is not hard to believe that the small dunes in crater Xn are composed of locally derived materials. If the dune sand was derived from outside of crater Xn, then it would have had to travel across one of the deep pits ringing crater Xn, and then across the flat crater floor to reach its current location. It is more probable that the dune sand is locally derived from pit and fracture walls, suggesting that the sand area has not traveled far from its source region. However, the Rabe Crater dune field is quite extensive ($\sim$50 $\times$ $\sim$35 km wide, up to 500 m high), and it covers a higher proportion of the crater floor than most other dune fields in Noachis Terra (see Figure 1). Yet the dune sand could easily fill the cavity volume of the pit, so it is possible that the Rabe Crater dune sand is derived entirely from pit materials. Furthermore, no accumulations of sand (sand streamers or drifts) are visible in images southeast of (or on) the Rabe Crater rim, the most plausible upwind source direction based on dune morphology. Although a distant sand source for the Rabe Crater dunes cannot be ruled out, a local source is consistent with observations.

[99] The hypothesis of a regional set of deposits may also be consistent with the observed correlation of crater size and nighttime temperatures. In most areas discussed above, craters with diameters less than $\sim$10 km all have floors that are dark (cool) in the nighttime IR mosaics. Most craters with diameters more than $\sim$20 km have floors that are bright (warm) in the nighttime IR mosaics. There are a few possible explanations for this pattern. One is that the larger bolides impacted farther into the southern highland surface, exposing underlying rock that has different physical properties than the more shallow rock exposed by smaller bolides. However, the exposure of layered material in pits within crater floors indicates that some amount of sediment has filled in the larger craters, suggesting that the nighttime bright material in the larger crater floors is not the original crater floor but more recent infill. For example, *Fenton et al.* [2005] estimated that Proctor Crater had $\sim$450 m of sediments filling its floor.

[100] Another explanation for the correlation of nighttime temperature and crater size relates to crater age. Most of the larger craters in Noachis Terra date to the Noachian epoch [*Petersen*, 1977], but some of the smaller craters may be much younger. It is possible that units such as those observed in Rabe Crater predate the formation of many of the younger craters in Noachis Terra. Thus the sedimentary units may never have been deposited in the smaller craters because they did not yet exist when deposition was taking place.

[101] Finally, the idea of widespread sedimentation across Noachis Terra may explain the many spots on the intercrater plains that appear bright (warm) in the nighttime IR mosaics. These nighttime-bright areas appear throughout most of the study area (see Figures 3c, 5c, 7c, and 9c). If the nighttime-bright units in Rabe Crater represent sedimentary units that were deposited over all or part of Noachis Terra, then the bright areas on the intercrater plains may be erosional remnants of similar (perhaps the same) units. The intercrater plains have poor coverage in MOC NA imagery, so that a systematic morphologic study of the night-bright spots is difficult. However, part of one of these bright spots is shown in the intercrater plains. The western edge of Figure 6b captures the eastern wall of a round mesa that is bright in the nighttime IR mosaics (see "5B" in Figure 5c). The top of the mesa has a dark mottled appearance that was interpreted as dark sand partly covering a bouldery or knobby surface. The wall of the mesa has bright lineations that may be outcrops of layers. The night-bright mesa has a texture similar to that of Rabe unit 4. If the night-bright areas in Noachis Terra are erosional remnants of sedimentary units, then they may be considered potential sources of dark dune sand. If so, then these nighttime-bright spots on the intercrater plains may be the sand source for the intercrater dune fields.

[102] If the nighttime-bright spots on the intercrater plains do represent erosional remnants of a formerly more extensive set of sedimentary layers, then it is possible to test the hypothesis that small ($<\sim$10 km diameter) craters postdate the deposition of these layers. There are few examples of THEMIS VIS images (not shown) of small nighttime-dark craters on the intercrater plains, but they do indicate that ejecta blankets of such craters overlap adjacent nighttime-bright spots. In some cases where ejecta blankets have been destroyed, it is clear that the small nighttime-dark craters formed from impacts into the nighttime-bright spots. However, there are a few places where the stratigraphy is unclear, and it is possible that nighttime-bright material on the intercrater plains buried some small nighttime-dark craters, and these craters are now exposed by erosion. It seems that in most cases, small nighttime-dark floored craters postdate the deposition of sedimentary materials on the intercrater plains.

[103] The concentration of dune fields in crater floors (rather than on the intercrater plains) may be dictated in part by the amount of remnant sedimentary layers still present within craters relative to that remaining on the intercrater plains. The amount of sedimentary material removed by erosion and the amount of cratering on that which still remains indicates that the formation of the sedimentary layers, and much of their subsequent erosion, took place long ago. These layers (and possibly the dunes) are not a product of recent climate changes that are considered responsible for polar layered terrains and other younger sediments.

[104] The hypothesis of regional sedimentation provides a potential source of sand for the dark dunes that is consistent with the lack of observed sand transport pathways in Noachis Terra. In this case, the sand source is a set of regional-wide deposits that may be exposed only locally (either in crater floors or on the intercrater plains), leading to dune formation not far from each set of local sources. A regional set of sedimentary layers would have draped the underlying topography, covering low-lying crater floors,

plains, and mountain ranges on the intercrater plains. The characteristics of these potentially sand-bearing sedimentary units provide information regarding their origin. For example, they could not be purely loess deposits, formed from dust that has settled from suspension, because the sand grains they contain would be too large to be carried into suspension in the first place. These units are also unlikely to be purely lacustrine deposits because of their potential extent out on the intercrater plains: while lakes may have formed in local topographic lows such as on crater floors, it is unlikely that lakes could have formed high up on the intercrater plains where the surface does not form a closed basin. It is possible that some of the deposits in some places may be either loess or ancient lake beds, but they cannot form the bulk of the sedimentary material. Other sources of material, such as volcanic ashfall or glacial till, cannot be ruled out by their spatial extent or the inclusion of sand grains in these deposits. In the future, better coverage with MOC NA and THEMIS images can help to connect a sequence of sedimentary units in one crater with those in another crater, or with those on the intercrater plains, allowing for further interpretation of sand sources.

5. Conclusions and Future Work

[105] Several areas in Noachis Terra, in the southern highlands of Mars, have been investigated with a number of data sets from different spacecraft. The goal was to determine sand transport pathways and potential sand sources for the many intracrater (and the few intercrater) dune fields in the area. The investigation led to the following observations and a hypothesis regarding the regional sedimentary history:

[106] Observations:

[107] 1. Unlike many terrestrial deserts, there is no sign of sand transport pathways upwind of the Noachis Terra dune fields leading to clear source regions.

[108] 2. Although most of the dune fields in Noachis Terra are located on the floors of the largest craters, there are two striking examples of dunes on the intercrater plains. In the first, a dune field has accumulated in a local topographic low. In the second, several dune fields are located in the Hellespontus Montes, against cliff walls that step eastward, down into Hellas Planitia.

[109] 3. Duneless areas that are dark in the MOC WA mosaic and bright (warm) in the daytime IR mosaic are interpreted as small (10–50 km wide) sand sheets. They are visible surrounding the dune fields in crater Np, on the intercrater plains, and potentially near Hellas. It is not clear in any images whether sand is being transported into or out of the dune field in the sand sheets. None of these features are visible in nighttime IR mosaics, suggesting that they are thermally thin (on the order of a few cm or less).

[110] 4. Most of the intercrater plains are relatively dark (cool) in the nighttime IR mosaics, but there are several small areas that are bright (warm). The nighttime IR images generally show much more spatial variation in surface properties than either the daytime IR mosaics or the MOC WA mosaics.

[111] 5. Several of the larger craters in Noachis Terra have pits eroded into their floors. Some of these pits, especially the large pit in Rabe Crater, show strata with varying textures and nighttime IR signatures.

[112] 6. MOC narrow-angle images reveal that the dunes in different dune fields generally show a similar set of two or three slipface orientations, with a few exceptions. This leads to the possibility that the dune-forming winds are created by regional (e.g., across Noachis Terra or larger), rather than local (e.g., on the scale of a single crater) processes.

[113] 7. The deep pit on the floor of Rabe Crater exposes a series of strata. From oldest to youngest: unit 1 is dark in nighttime IR mosaics, easily erodible, and untextured; unit 2 is relatively thin, layered and blocky, and bright in nighttime IR mosaics; unit 3 is composed of two or three layers with an etched appearance and it is bright in nighttime IR mosaics, and unit 4 has a rough, blocky texture and it is bright in nighttime IR mosaics. Pit walls in crater Xn have characteristics very similar to units 1 and 2 in Rabe Crater.

[114] 8. Crater Xn appears to have been nearly completely filled in with sediments at some unknown point in the past. Since that time, arcuate pits ringing the inside of the crater rim have formed, indicating that a large amount of material has eroded from this area. Dunes within a central pit in crater Xn were likely formed from materials eroding from the pit walls; it seems unlikely that sand was transported over several different deep pits from outside of crater Xn.

[115] Hypothesis of regional deposition: There were a series of region-wide depositional events that are currently exposed as sedimentary layers in the pit walls of craters in Noachis Terra. Some of these sedimentary layers are shedding dark sand that has formed into the dark dunes of Noachis Terra.

[116] Implications of the hypothesis of regional deposition:

[117] 1. At some unknown (but not recent) point in the Martian past, an enormous amount of material accumulated on the heavily cratered terrain of Noachis Terra, perhaps separated by periods of inactivity or erosion. The sediments are unlikely to be dominated by lacustrine and loess deposits; glacial till and volcanic ash provide a better match to the observed characteristics of the layers. Since that time and up to the present, the surface has been dominated by erosion that has removed much of the previously deposited material.

[118] 2. The lack of observable sand transport pathways suggests that such pathways are very short, ruling out a distant source of sand. Dunes located on the intercrater plains probably have sand sources nearby on the intercrater plains. Dunes located on crater floors probably have sand sources either within the crater or near the crater on the intercrater plains (or both). In this case, the dune sources are a combination of regional and local types: sand may be eroding from a widespread source that only outcrops locally. Possible examples of such layers are Rabe Crater units 1 and 3.

[119] 3. Larger craters ($>\sim$20 km diameter) have floors that are bright (warm) in the nighttime IR mosaics. Smaller craters ($<\sim$10 km diameter) have floors that are dark (cool) in the nighttime IR mosaics. Intermediate craters (10–20 km diameter) have floors that are partially bright and partially dark in nighttime IR mosaics. This relationship

is broken only in one crater near the Hellas rim. This progression of crater sizes and relative floor temperatures may relate to crater ages and the timing of sediment deposition: smaller craters with nighttime-dark floors may have formed after the nighttime-bright sediments were deposited in larger, older craters.

[120] 4. Not all of the units observed in Rabe Crater are present in all crater pits. It may be that some of the Rabe Crater units were not deposited across all of Noachis Terra, or that they were deposited and have since been eroded away in some places.

[121] 5. Spots on the intercrater plains that are bright in the nighttime IR mosaic and have characteristics similar to the Rabe Crater units may be erosional remnants of these (or similar) units. If this is the case, then these night-bright patches may be sand sources for the intercrater dune fields.

[122] In order to further test this hypothesis, more data is necessary. This is especially true for nighttime-bright patches on the intercrater plains that are currently poorly sampled by both THEMIS VIS and MOC NA; better coverage of both of these data sets could prove helpful. Other data, such as the compositional information provided by TES and THEMIS, may be used to better correlate the Rabe units with similar units elsewhere in Noachis Terra. With better image coverage and further study, a full stratigraphic history of sedimentary deposits can be constructed for Noachis Terra, leading to a better understanding of the erosion, transport, and deposition of fine-grained material on the surface of Mars.

[123] **Acknowledgments.** The author would like to give thanks to the THEMIS team and Trent Hare for providing tools and data necessary for this work. In addition, the author thanks Kelly Bender and reviewers Matthew Balme and Nick Lancaster for helpful comments and suggestions.

References

Aben, L. K. (2003), Compositional and thermophysical analysis of Martian aeolian dunes, M.S. thesis, 117 pp., Ariz. State Univ., Tempe.

Bagnold, R. A. (1941), *The Physics of Blown Sand and Desert Dunes*, Methuen, New York.

Breed, C. S. (1977), Terrestrial analogs of the Hellespontus Dunes, Mars, *Icarus*, *30*, 326–340.

Breed, C. S., M. J. Grolier, and J. F. McCauley (1979), Morphology and distribution of common "sand" dunes on Mars: Comparison with the Earth, *J. Geophys. Res.*, *84*, 8183–8204.

Bridges, N. T., R. Greeley, A. F. C. Haldemann, K. E. Herkenhoff, M. Kraft, T. J. Parker, and A. W. Ward (1999), Ventifacts at the Pathfinder landing site, *J. Geophys. Res.*, *104*(E4), 8595–9615.

Bridges, N. T., R. Greeley, E. Eddlemon, J. E. Laity, C. Meyer, J. Phoreman, and B. R. White (2003), Martian and terrestrial rock abrasion from wind tunnel and field studies, *Lunar Planet. Sci.*, *XXXIV*, Abstract 1766.

Byrne, S., and B. C. Murray (2002), North polar stratigraphy and the paleoerg of Mars, *J. Geophys. Res.*, *107*(E6), 5044, doi:10.1029/2001JE001615.

Calkin, P. E., and R. H. Rutford (1974), The sand dunes of Victoria Valley, Antarctica, *Geogr. Rev.*, *64*, 189–216.

Christensen, P. R. (1983), Eolian intracrater deposits on Mars: Physical properties and global distribution, *Icarus*, *56*, 496–518.

Clarke, M. L., and H. M. Rendell (1998), Climate change impacts on sand supply and the formation of desert sand dunes in the south-west U.S.A., *J. Arid. Environ.*, *39*, 517–531.

Cutts, J. A., and R. S. U. Smith (1973), Aeolian deposits and dunes on Mars, *J. Geophys. Res.*, *78*, 4139–4154.

Edgett, K. S., and N. Lancaster (1993), Volcaniclastic aeolian dunes: Terrestrial examples and application to Martian sands, *J. Arid Environ.*, *25*, 271–297.

Edgett, K. S., and M. C. Malin (2000a), New views of Mars eolian activity, materials, and surface properties: Three vignettes from the Mars Global Surveyor Mars Orbiter Camera, *J. Geophys. Res.*, *105*, 1623–1650.

Edgett, K. S., and M. C. Malin (2000b), Examples of Martian sandstone: Indurated, lithified and cratered eolian dunes in MGS MOC images, *Lunar Planet. Sci.*, *XXXI*, Abstract 1071.

Edgett, K. S., R. M. E. Williams, M. C. Malin, B. A. Cantor, and P. C. Thomas (2003), Mars landscape evolution: Influence of stratigraphy on geomorphology in the north polar region, *Geomorphology*, *52*(3–4), 289–297.

Fenton, L. K., and M. I. Richardson (2001), Martian surface winds: Insensitivity to orbital changes and implications for aeolian processes, *J. Geophys. Res.*, *106*(E12), 32,885–32,902.

Fenton, L. K., J. L. Bandfield, and A. W. Ward (2003), Aeolian processes in Proctor Crater on Mars: Sedimentary history as analyzed from multiple data sets, *J. Geophys. Res.*, *108*(E12), 5129, doi:10.1029/2002JE002015.

Fenton, L. K., A. D. Toigo, and M. I. Richardson (2005), Aeolian processes in Proctor Crater on Mars: Mesoscale modeling of dune-forming winds, *J. Geophys. Res.*, *110*, E06005, doi:10.1029/2004JE002309.

Fryberger, S. G. (1979), Dune forms and wind regime, *U.S. Geol. Surv. Prof. Pap.*, *1052*, 137–170.

Fryberger, S. G., and T. S. Ahlbrandt (1979), Mechanisms for the formation of eolian sand seas, *Z. Geomorphol. NF*, *23*(4), 440–460.

Gorelick, N. S., M. Weiss-Malik, B. Steinberg, and S. Anwar (2003), JMARS: A multimission data fusion application, *Lunar Planet. Sci.*, *XXXIV*, Abstract 2057.

Greeley, R., N. Lancaster, S. Lee, and P. Thomas (1992), Martian aeolian processes, sediments, and features, in *Mars*, edited by H. H. Kieffer et al., pp. 730–766, Univ. of Ariz. Press, Tucson.

Greeley, R., A. Skypeck, and J. B. Pollack (1993), Martian aeolian features and deposits: Comparisons with general circulation model results, *J. Geophys. Res.*, *98*, 3183–3196.

Greeley, R., M. Kraft, R. Sullivan, G. Wilson, N. Bridges, K. Herkenhoff, R. O. Kuzmin, M. Malin, and W. Ward (1999), Aeolian features and processes at the Mars Pathfinder landing site, *J. Geophys. Res.*, *104*(E4), 8573–8584.

Haberle, R. M., J. R. Murphy, and J. Schaeffer (2003), Orbital change experiments with a Mars general circulation model, *Icarus*, *161*, 66–89.

Hartmann, W. K., J. Anguita, M. A. de la Casa, D. C. Berman, and E. V. Ryan (2001), Martian cratering 7: The role of impact gardening, *Icarus*, *149*, 37–53.

Isarin, R. F. B., H. Renssen, and E. A. Koster (1997), Surface wind climate during the Younger Dryas in Europe as inferred from aeolian records an model simulations, *Palaeogeogr. Palaeoclimatol. Palaeoecol.*, *134*, 127–148.

Joshi, M. M., R. M. Haberle, J. R. Barnes, J. R. Murphy, and J. Schaeffer (1997), Low-level jets in the NASA Ames Mars general circulation model, *J. Geophys. Res.*, *102*(E3), 6511–6523.

Kocurek, G., and N. Lancaster (1999), Aeolian sediment states: Theory and Mojave Desert Kelso Dune field example, *Sedimentology*, *46*(3), 505–516.

Kreslavsky, M. A., and J. W. Head III (2000), Kilometer-scale roughness of Mars: Results from MOLA data analysis, *J. Geophys. Res.*, *105*(E11), 26,695–26,711.

Lancaster, N., and R. Greeley (1987), Mars: Morphology of southern hemisphere intracrater dunefields, *NASA Tech. Memo.*, *89810*, 264–265.

Lancaster, N., G. Kocurek, A. Singhvi, V. Pandey, M. Deynoux, J.-F. Ghienne, and K. Lô (2002), Late Pleistocene and Holocene dune activity and wind regimes in the western Sahara Desert of Mauritania, *Geology*, *30*(11), 991–994.

Livingstone, I., and A. Warren (1996), *Aeolian Geomorphology*, 211 pp., Addison-Wesley, Boston, Mass.

Mainguet, M. (1978), The influence of trade winds, local air-masses and topographic obstacles on the aeolian movement of sand particles and the origin and distribution of dunes and ergs in the Sahara and Australia, *Geoforum*, *9*, 17–28.

Mainguet, M. M., and F. El-Baz (1986), Deciphering wind directions from dune orientations in space images of deserts and semiarid lands, in *Proceedings of the 20th International Symposium on Remote Sensing of the Environment, 4–10 December 1996, Nairobi, Kenya*, pp. 115–125, Environ. Res. Inst. of Mich., Ann Arbor.

Malin, M. C., and K. S. Edgett (2000), Sedimentary rocks of early Mars, *Science*, *290*, 1927–1937.

Malin, M. C., and K. S. Edgett (2001), Mars Global Surveyor Mars Orbiter Camera: Interplanetary cruise through primary mission, *J. Geophys. Res.*, *106*(E10), 23,429–23,570.

McCauley, J. F., M. J. Grolier, and C. S. Breed (1977), Yardangs of Peru and other desert regions, *U.S. Geol. Surv. Interagency Rep. Astrogeol.*, *81*.

McDonald, R. R., and R. S. Anderson (1995), Experimental verification of aeolian saltation and lee side deposition models, *Sedimentology*, *42*, 39–56.

McKee, E. D. (1979), Introduction to a study of global sand seas, in *A Study of Global Sand Seas*, *U. S. Geol. Surv. Prof. Pap.*, *1052*, 1–19.

Muhs, D. R., T. W. Stafford, S. D. Cowherd, S. A. Mahan, R. Kihl, P. B. Maat, C. A. Bush, and J. Nehring (1996), Origin of the late Quaternary dune fields of northeastern Colorado, *Geomorphology*, *17*, 129–149.

Nickling, W. G., C. McKenna Neuman, and N. Lancaster (2002), Grainfall processes in the lee of transverse dunes, Silver Peak, Nevada, *Sedimentology*, *49*, 191–209.

Petersen, J. E. (1977), Geologic map of the Noachis Quadrangle of Mars, *U.S. Geol. Surv. Misc. Geol. Invest. Map*, *I-910*.

Putzig, T. E., M. T. Mellon, K. A. Kretke, and R. E. Arvidson (2005), Global thermal inertia and surface properties of Mars from the MGS mapping mission, *Icarus*, *173*, 325–341.

Ramsey, M. S., P. R. Christensen, N. Lancaster, and D. A. Howard (1999), Identification of sand sources and transport pathways at the Kelso Dunes, California, using thermal infrared remote sensing, *Geol. Soc. Am. Bull.*, *111*, 646–662.

Roark, J. H., and H. V. Frey (2001), GRIDVIEW: Recent improvements in research and education software for exploring Mars topography, *Lunar Planet. Sci.*, *XXXII*, Abstract 1618.

Roark, J. H., H. V. Frey, and S. Sakimoto (2000), Interactive graphics tools for analysis of MOLA and other data, *Lunar Planet. Sci.*, *XXXI*, Abstract 2026.

Sharp, R. P. (1966), Kelso Dunes, Mojave Desert, California, *Geol. Soc. Am. Bull.*, *77*, 1045–1074.

Sullivan, R. J., et al. (2005), Aeolian processes at the Mars Exploration Rover Opportunity landing site, *Lunar Planet. Sci.*, *XXXVI*, Abstract 1942.

Tanaka, K. L. (2000), Dust and ice deposition in the Martian geologic record, *Icarus*, *144*, 254–266.

Thomas, P., and J. Veverka (1979), Seasonal and secular variation of wind streaks on Mars: An analysis of Mariner 9 and Viking Data, *J. Geophys. Res.*, *84*, 8131–8146.

Thomas, P., J. Veverka, D. Gineris, and L. Wong (1984), "Dust" streaks on Mars, *Icarus*, *60*, 161–179.

Ward, A. W., K. B. Doyle, P. J. Helm, M. K. Weisman, and N. E. Witbeck (1985), Global map of eolian features on Mars, *J. Geophys. Res.*, *90*, 2038–2056.

Ward, W. R. (1992), Long-term orbital and spin dynamics, in *Mars*, edited by H. H. Kieffer et al., pp. 298–320, Univ. of Ariz. Press, Tucson.

White, B. R. (1979), Soil transport by winds on Mars, *J. Geophys. Res.*, *84*, 4643–4651.

Wilson, S. A., J. R. Zimbelman, and S. H. Williams (2003), Large aeolian ripples: Extrapolations from Earth to Mars, *Lunar Planet. Sci.*, *XXXIV*, Abstract 1862.

Zimbelman, J. R., S. H. Williams, and V. P. Tchakerian (1995), Sand transport paths in the Mojave Desert, southwestern United States, in *Desert Aeolian Processes*, edited by V. P. Tchakerian, pp. 101–130, St. Edmundsbury, Bury St. Edmonds, UK.

L. K. Fenton, Department of Geology, Arizona State University, Mail Code 1404, Tempe, AZ 85287, USA. (lkfenton@asu.edu)